JOURNAL OF GEOPHYSICAL RESEARCH, VOL. 91, NO. C2, PAGES 2616–2632, FEBRUARY 15, 1986

Short Surface Waves With Growth and Dissipation

JEROME SMITH

Scripps Institution of Oceanography, La Jolla, California

The modulation of surface waves by larger-scale flows is central to many forms of remote imaging of the sea surface yet is an incompletely understood process. An excellent example is the modulation of short waves by long ones (e.g., by swell). Observed modulations are of the order of 10 times the long-wave steepness, decrease with both the long-wave frequency and windspeed, and have stable phase, with maximum short-wave amplitudes just forward of the long-wave crests. Assuming a balance between propagation, growth, and drift-enhanced dissipation, the short-wave modulations arise owing to (1) direct straining by the long-wave orbital motion, (2) straining of the wind drift layer (modulating the dissipation rate), (3) variations of the apparent gravity in the short-wave frame, and (4) induced variations of the applied wind stress (affecting both the short-wave growth and the drift-enhanced dissipation). As modeled here, only the last (stress variation) can reproduce the observed wind speed and frequency dependence. In addition, the drift layer and the short waves are closely matched, suggesting direct coupling. The implied fractional modulation of stress is of the order of 20 times the long-wave steepness.

1. Introduction

In recent years, many interesting and beautiful images of the ocean surface have begun to appear, owing largely to the development of techniques employing electromagnetic backscatter. Under many circumstances, this backscatter results from resonant Bragg scattering from freely propagating surface waves [*Wright*, 1968; *Stewart and Joy*, 1974; *Valenzuela*, 1978, 1980; *Alpers and Hasselmann*, 1978; *Plant and Wright*, 1980; *Plant and Keller*, 1983, etc.]. In the case of SAR or other techniques using GHz-frequency radars, the Bragg scatterers are gravity-capillary waves with wavelengths in the range 1–50 cm or so. The variations in backscattered intensity largely trace the hydrodynamic behavior of these short waves. To the extent that the short-wave amplitudes respond to the winds and to the currents induced by swell, internal waves, bottom topography, etc., such larger-scale structures are imaged.

An attraction of these images is the possibility of continual global coverage of winds, waves, and currents, which could ostensibly become available via satellite. The strength of this attraction makes it desirable to attempt a hydrodynamic description of the short-wave behavior, although in some respects it is somewhat premature. In order to produce results which can be compared to existing data, many assumptions must be made, of which many are little more than speculation. Nevertheless, the dynamic framework provides some insight into which of these ill-known factors are most likely to be important and may also provide insight as to how to estimate them better.

Perhaps the most careful, complete, and thus theoretically exacting set of measurements to date concern the modulation of short waves by swell. It is a long-standing observation that short surface waves have greater amplitudes (or mean steepness) slightly forward of long-wave crests [*Cox*, 1958; *Keller and Wright*, 1975; *Wright et al.*, 1980; *Plant et al.*, 1983; *Keller et al.*, 1985; etc.]. A particular attraction of radar backscatter in detecting amplitudes of such short surface waves is the fact that Doppler shifting has no direct effect on the scale of the waves detected and is, in addition, measurable by the technique, providing a direct estimate of the long-wave orbital velocity. Optical measurements share the quality of "Doppler independence" for the short waves [*Monaldo and Kasevich*, 1981, 1982]; however, nonlinear shading by the short-wave roughness itself may confuse the estimates of long-wave slope and phase. In contrast, measurements by a wire or laser slope meter (for example) are smeared over a large band of wavelengths, owing especially to the substantial orbital velocities of the larger waves. Here, the case of short waves modulated by longer ones is used to study some implications of a model based on a local balance between the advection, growth, and dissipation of such short waves; in view of the above considerations, the results will be compared primarily with the radar measurements.

To translate observations into quantitative information about the large-scale flow, appeals have been made to relaxation of the short waves toward an equilibrium level, versus the tendency of perturbing currents (or winds) to drive them off equilibrium [*Keller and Wright*, 1975; *Valenzuela and Wright*, 1979; *Alpers and Hemmings*, 1984, etc.]. A tidy summary of our present understanding of this equilibrium, including generation, dissipation, and wave-wave interactions, is given by *Phillips* [1984] (see also *Plant* [1980]). In the relaxation approach, discussion of the physics of short-wave generation and dissipation is (quite intentionally) avoided. The intention here is not to replace the relaxation concept but simply to see what may be learned by applying a set of plausible, physically based assumptions.

The salient features of the observed short-wave modulations are more or less summarized by the results shown in Figures 1 and 2 [from *Plant et al.*, 1983]. These show measured "modulation transfer functions" (MTFs) for two wavelengths: roughly, 2.1-cm waves (Figure 1) and 12-cm (Figure 2). Although the MTFs (defined as backscatter intensity modulations divided by the long-wave steepness, U^L/C^L) include other effects as well (e.g., tilting and range variations), we are assured by the experimenters that the major characteristics shown reflect the modulation of the short waves themselves, at a (more or less) fixed wavelength. Note that there is a consistent decrease in the magnitude of the modulation with long-wave (driving) frequency and that the phases of the modulations are quite stable, around 0° to 30° ahead of the long-wave crests. Also, note that the X band (2.1 cm) modulations decrease with increasing winds (over the range 5 to 14 m/s), while the L band (12 cm) modulations are insensitive to wind speed (in the range 7 to 15 m/s).

Here, a two-scale analysis, based on the "action equation" [*Bretherton and Garrett*, 1969] modified to include direct gen-

Paper number 5C0778.
0148-0227/86/005C-0778$05.00

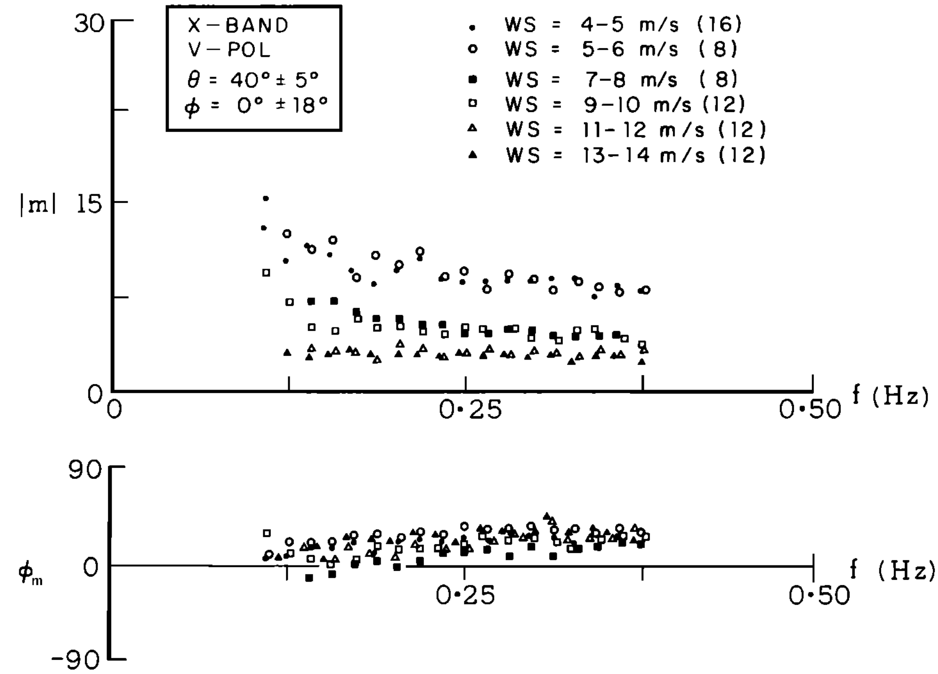

Fig. 1. MTF versus long-wave frequency for 2.1-cm waves (X band radar, vertical polarization), for various wind speeds. The MTF is the ratio of the correlated backscatter intensity modulations to long-wave steepness. Numbers in parentheses are numbers of files averaged; each file is an average of 20 spectra (reproduced from *Plant et al.* [1983]; see the source for details).

eration and dissipation (cf. *Garrett and Smith*, 1976], is used to trace the evolution of a short-wave "spectral band" or "packet," propagating over long gravity waves. This analysis presumes that the long and short waves are sufficiently different in scale to apply the "slowly varying hypothesis" (i.e., the Wentzel-Kramers-Brillouin or WKB assumption). For simplicity, a monochromatic long wave is considered, and ultimately only the first-order results (in long-wave steepness) are pursued for comparison with experiment. The focus here is on the local hydrodynamics of the short-wave modulations; in particular, nonlinear transfer of energy to or from other spectral components is neglected in comparison to the direct generation, dissipation, and advection (straining) of the short waves. This "local balance" hypothesis is inspired by the rather strong generation of waves near the minimum phase speed (say, 1–10 cm long), as demonstrated by *Larson and Wright* [1975] and *Plant and Wright* [1977].

The details of short-wave growth and dissipation in the presence of long waves are buried in the strongly nonlinear, coupled shear flow between the air and sea [e.g., *Valenzuela*, 1976]. Worse, the variation in surface roughness introduced by the short waves is itself of primary importance there [e.g., *Gent and Taylor*, 1976; *Townsend*, 1980; *Landahl et al.*, 1981]. However, theoretical analyses of this problem more or less agree that the applied shearstress is greatest somewhere near the long-wave crests. Since the long waves are rapidly overtaking the short ones, maximal short-wave growth at long-wave crests would, by itself, lead to short-wave maxima toward the rear face of the longer peaks, contrary to observation; by the same reasoning, maximal dissipation near long-wave crests would tend to move the short-wave maxima forward.

Estimation of a short-wave dissipation rate is achieved by combining (1) a "narrow-band" theory for breaking waves, yielding a fraction of energy dissipated per wave cycle [*Longuet-Higgins*, 1 ʕ9*a*] and (2) a maximum steepness criterion including th‹ effects of "wind drift" [*Phillips and Banner*, 1974] and partial advection of the short waves [cf. *Stewart and Joy*, 1974; *Plant and Wright*, 1980]. To this end, evolution of the wind drift is reviewed [cf. *Phillips*, 1977; *Longuet-Higgins*, 1969*b*], and a "turbulent readjustment" is modeled via relaxation. The effects of a varying tangential wind stress on the drift (and hence on short-wave dissipation) are modeled separately.

Finally, to compare the results to radar requires consideration of "spectral shifting terms", i.e., variations in backscatter intensity due to (1) changes in the intrinsic wave number due to straining, Δk^{packet}, and (2) changes in the detected wave number due to surface tilting by the long waves, Δk^{Bragg}. These "corrections" depend critically on the spectral form $F(k)$, which may be ill known, especially for short waves near the "viscous cutoff." While an attempt is made to accommodate the first of these corrections (i.e., to describe the apparent variations in amplitude at a fixed wave number), the second is not pursued (there are also corrections for the variation in range and in sensitivity versus tilt, etc. [see *Plant et al.*, 1983]. The variations in wave number due to long-wave straining induce variations in measured amplitude via both the spectral slope and dynamics: As the energy in an adjacent spectral band is brought into "view" by the changing wave number, the energy itself changes so as to conserve the action of the component waves. In view of this, it is convenient to evaluate this "Boltzman transport" term via an action spectrum.

The model results are fairly sensitive to two aspects of the wind drift. Comparison of model and observed short-wave spectra indicates the drift layer to have a roughness length scale which increases with increasing wind. Comparison of model and observed short-wave modulations supports this and also indicates that the time scale of drift evolution must be comparable to that of the short waves.

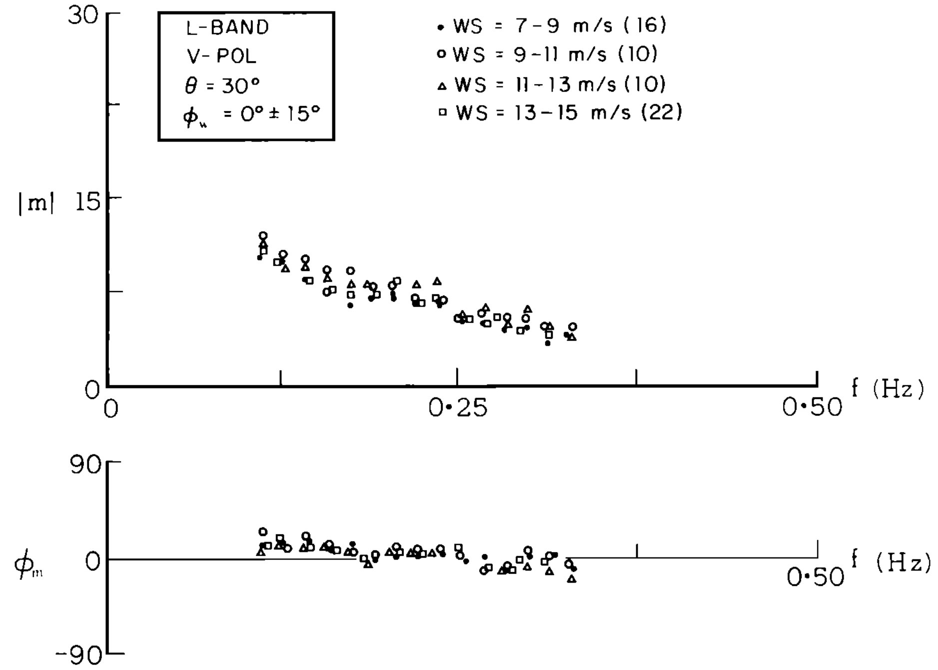

Fig. 2. MTF versus long-wave frequency for 12-cm waves (L band radar, vertical polarization), for various wind speeds (as in Figure 1; reproduced from *Plant et al.* [1983]).

2. SHORT-WAVE EQUATIONS

Moving with the "advection velocity" $\mathbf{U}$ of the water below the short waves, the dispersion relation between short-wave "intrinsic frequency" ω and wave number k is modified by accelerations due to the long waves:

$$\omega = (g'K + Tk^3)^{1/2} \tag{1}$$

where T is the kinematic surface tension (about 72 cm^3/s^2 for clean seawater near 15°C) and $g' = |\mathbf{g} + D_t\mathbf{U}|$ is an effective gravity (here, D_t is the material derivative, $(\partial/\partial t + \mathbf{U} \cdot \nabla)$). All but the vertical component of acceleration, $\ddot{Z} \equiv D_t{}^2 Z$ (where Z is the mean surface displacement, averaged over the short-wave phase), will be neglected, and even this is unimportant except in determination of intrinsic frequency (and hence phase speed). Surface tension T may also be modulated (e.g., because of distortion and compression of surface contaminants [cf. *Lange and Huhnerfuss*, 1984]), but no attempt is made here to model this.

Variations in short-wave number $\mathbf{k}$ are described by [e.g., *Phillips*, 1977]:

$$\frac{\partial \mathbf{k}}{\partial t} + \nabla_H(\omega + \mathbf{k} \cdot \mathbf{U}) = 0 \tag{2}$$

The short-wave advection velocity $\mathbf{U}$ includes both long-wave orbital velocity $\mathbf{U}^L$ and the part of the surface wind drift which advects the short waves bodily, $\mathbf{U}^a$. For waves near the minimum phase speed (especially) the depth of the wind-induced "viscous sublayer" may not be negligible. The advective drift velocity $\mathbf{U}^a$ can be estimated from a detailed velocity profile $\mathbf{U}^D(z)$ (averaged over the short-wave phase) provided the shear $\partial\mathbf{U}^D/\partial z$ is not too large in comparison to ω [*Stewart and Joy*, 1974]:

$$\mathbf{U}^a = 2k \int_{-\infty}^{0} \mathbf{U}^D(z)\, e^{2kz}\, dz \tag{3}$$

(see also *Plant and Wright* [1980]). The remaining surface flow $\mathbf{q} \equiv \mathbf{U}^D(Z) - \mathbf{U}^a$ is important to the short-wave dissipation model, to be discussed in section 3.

The short-wave "intrinsic energy" E is evaluated in this frame:

$$E \approx \rho\langle(g'\zeta + T\nabla^2\zeta)\zeta\rangle \approx (\rho\omega^2/k^3)\tfrac{1}{2}s^2 \tag{4}$$

where ρ is the water density, ζ is the short-wave-induced surface displacement (from Z), the angle brackets ($\langle\ \rangle$) denote averaging over short-wave phase only, and $s = ak$ (where a is amplitude) is a measure of short-wave steepness.

Variations in the short-wave energy are traced by conservation of action [*Bretherton and Garrett*, 1969], defined as the ratio of intrinsic energy to frequency:

$$A = E/\omega \approx (\rho\omega/k^3)\tfrac{1}{2}s^2 \tag{5}$$

Here, the action equation is modified to include growth G and dissipation D:

$$\frac{\partial A}{\partial t} + \nabla_H \cdot [(\mathbf{U} + \mathbf{c}^{gs})A] = (G - D)A \tag{6}$$

where $\mathbf{c}^{gs}$ is the short-wave group velocity. The non-conservative terms G and D appear here multiplied by A to emphasize at least proportionality to A and also to simplify the form of the solution; in particular, the dissipation D is expected to have additional, stronger A dependence. An effect of including G and D is that no singularities occur: For example, when the net action-flux converges toward a turning point, the input of action due to the convergence can always be accounted for by an excess of dissipation over growth. Direct forcing by random pressure fluctuations and action transfer from other scales are both neglected in the above equation in comparison to the direct forcing by D and G.

The advection velocity U^a is no greater than a few percent of the windspeed, while the long-wave phase speeds may reasonably be taken as being comparable to the windspeed; thus the analysis is restricted to the case $U^a/C^L \ll 1$. Also, considering short waves to the gravity side of $c^{\min}$, the assumption

$K \ll k$ (where K is the long-wave number) implies $c^{gs} \ll C^L$. Although U^a and c^{gs} are therefore safely ignored here, their effect on dissipation via q may be important.

To simplify presentation, envision a monochromatic long wave, propagating in the $+x$ direction, and shift to a reference frame moving with the long-wave phase speed, C^L (the long-wave "steady frame"). In this frame the long-wave-induced forcing becomes a function of x only, and so the resulting "short-wave-averaged" quantities (A, k, etc.) are also functions of x only. Applying the last two approximations,

$$\frac{\partial}{\partial x}[(C^L - U^L)A] = (D - G)A \tag{7}$$

Neglecting U^a and c^{gs} also helps simplify evaluation of the short-wave number $\mathbf{k}$. Using the chain rule to evaluate ω in (2) via the dispersion relation (1), the result for the x component k_x is

$$(C^L - U^L)\frac{\partial k_x}{\partial x} = k_x \frac{\partial U^L}{\partial x} + \tfrac{1}{2}(k/\omega)\frac{\partial \ddot{Z}}{\partial x} + \tfrac{1}{2}(k^3/\omega)\frac{\partial T}{\partial x} \tag{8}$$

As noted by *Garrett and Smith* [1976], the second (acceleration) term is at most of the order of $\frac{1}{2}(\Omega/\omega)\sec\theta_s$ in relation to the first (Doppler) term, where Ω is the long-wave frequency and θ_s is the angle between the short- and long-wave propagation directions (measured where $U^L = 0$). For $\Omega \ll \omega$ this term is negligible except in the extreme case where $\theta_s \to \pm\pi/2$. For $Tk^2 \leq g$ the same argument justifies neglect of the variations in T as well (for comparable fractional modulation of T versus g). Thus to a fair approximation,

$$\mathbf{k} = k_0\left(\frac{\cos\theta_s}{1 - U^L/C^L}, \sin\theta_s\right) \tag{9}$$

The major assumptions employed so far are (1) $\Omega \ll \omega$ (and hence $K \ll k$ and $c^{gs} \ll C^L$ as well), (2) the surface drift velocity is much smaller than the long-wave phase speed, and (3) the effects of all waves other than the band of short waves and the long waves considered are negligible.

Small Modulations

For simplicity, the long-wave orbital velocity is now expanded in terms of simple harmonics:

$$\mathbf{U}^L = \mathrm{Re}\,\{\varepsilon\mathbf{C}_1 e^{i\chi} + \varepsilon^2\mathbf{C}_2 e^{i2\chi} + \cdots\} \tag{10}$$

where ε is the long-wave steepness parameter $\mathbf{C}_1 \equiv (C^L, 0)$ and $\chi \equiv Kx - \Omega t$ is the long-wave phase function. From (9), the first-order variations in short-wave number are simply $k_{1x} = k_{0x}$ and $k_{1y} = 0$. The first order variation of the short-wave frequency, neglecting variations in surface tension, becomes

$$\omega_1\omega_0 \approx (c_0^{gs}/c_0)\cos^2\theta_s - g/(2c_0\omega_0) \tag{11}$$

where $c_0 = \omega_0/k_0$ is the mean phase speed of the short waves. Next, the short-wave action is expanded in powers of ε:

$$A(\chi) = A_0 + \varepsilon A_1 e^{i\chi} + O(\varepsilon^2) \tag{12}$$

Also, Taylor expansion of G and D in terms of both A and U^L yields

$$G = G_0 + \varepsilon\left(A_1\frac{\partial G}{\partial A} + C^L e^{i\chi}\frac{\partial G}{\partial U^L}\right) + O(\varepsilon^2) \tag{13}$$

$$D = D_0 + \varepsilon\left(A_1\frac{\partial D}{\partial A} + C^L e^{i\chi}\frac{\partial D}{\partial U^L}\right) + O(\varepsilon^2) \tag{14}$$

where the derivatives are evaluated with $A = A_0$ and $U^L = 0$.

Gathering terms of similar order in ε, the zero-order action equation yields $D_0 = G_0$, while the order ε equation is

$$C^L\frac{\partial}{\partial x}(A_1 e^{i\chi}) - R^A(A_1 e^{i\chi}) = \left[\frac{\partial}{\partial x}(C^L e^{i\chi}) - F^A e^{i\chi}\right]A_0 \tag{15}$$

where

$$R^A = \frac{\partial(D - G)}{\partial A} \tag{16}$$

and

$$F^A = (C^L/A_0)\frac{\partial(G - D)}{\partial U^L} \tag{17}$$

Solution of the above yields

$$A_1 = A_0\left(\frac{F^A - i\Omega}{R^A - i\Omega}\right) \tag{18}$$

Physically, the zeroth-order equation states that overall dissipation balances overall growth, while at order ε there is a damped response (with relaxation rate R^A) to the harmonic forcing due to straining ($-i\Omega$) and to variations in the dissipative balance (F^A). Note that for the "conservative case" (where R^A and $F^A \to 0$), $A_1 \to A_0$, consistent with previous results [e.g., *Garrett and Smith*, 1976]. The MTF (of *Plant et al.* [1983], etc.) corresponds roughly to A_1/A_0.

Growth

The short-wave growth rate suggested by *Plant* [1980, 1982] is based on radar measurements of the growth of centimetric waves in a wind-wave tank (but the angular dependence is uncertain [*Larson and Wright*, 1975; *Plant and Wright*, 1977]):

$$G \approx 33(\boldsymbol{\tau}\cdot\mathbf{k})/\rho c = 33(w_*^2k^2\omega^{-1})\cos(\theta_s - \theta_w) \tag{19}$$

where $\boldsymbol{\tau}$ is the wind stress, ρ is the water density, and w_* is the water friction velocity. In order to better fit the data to the capillary side of $c^{\min}$ (near $k = 3.7\ \mathrm{cm}^{-1}$) an additional factor $(1 + Tk^2/g)^{-1/2}$ is here applied to G (see, for example, Figure 1 of *Plant* [1982]).

It seems reasonable to suppose that the variations in shear stress induced by the long waves [cf. *Gent and Taylor*, 1976; *Townsend*, 1980; *Landahl et al.*, 1981] are transmitted, at finer scale, to the growth rate of the short waves as well as to the drift layer. The induced variation of shear stress is given the form (neglecting veering)

$$\boldsymbol{\tau} = \boldsymbol{\tau}_0\,\mathrm{Re}\,[1 + \varepsilon t_1 e^{i\chi} + \cdots] \tag{20}$$

where the magnitude of t_1 could be anything from 0 to 20 or so. For simplicity, the analysis is carried through for t_1 all real (i.e., maximum stress at the long-wave crests); extension to complex values is trivial.

Some recent measurements of velocity near the moving sea surface (between 30 and 274 cm above the free surface) indicate relatively little variation in windspeed with long-wave phase [*Hsiao and Shemdin*, 1983]. This is especially surprising, since it runs counter to both the results of theoretical calculations (e.g., those mentioned above) and to the extensive lore of sailors of small craft on the ocean. *Hsiao and Shemdin* [1983] continue with the speculation that this also implies little variation in stress. However, models of wind flow over a wavy surface with constant stress at the surface display substantial velocity variations. A simple momentum-based argument applied within the boundary layer therefore implies in order to reduce the velocity fluctuations there must be substantial variations in the stress applied at the surface. In the absence of any direct measurements of stress variation with long-wave phase it is regarded here as essentially a free parameter of the model.

The net variation in short-wave growth rate is obtained by adding the first-order variations due to the varying applied stress to those due to changes in **k** and g:

$$G_1 = C^L \frac{\partial G}{\partial U^L} = G_1{}^{\tau} + G_1{}^{k} + G_1{}^{g} \tag{21}$$

where

$$G_1{}^{\tau} = t_1 G_0 \tag{22}$$

$$G_1{}^{k} = G_0\left(\frac{\cos\theta_w \cos\theta_s}{\cos(\theta_w - \theta_s)} + \cos^2\theta_s[1 - c_0{}^g/c_0 - Tk_0{}^2/(g + Tk_0{}^2)]\right) \tag{23}$$

and

$$G_1{}^{g} = \tfrac{1}{2}(gk_0\omega_0{}^{-2} - Tk_0{}^2/(g + Tk_0{}^2))G_0 \tag{24}$$

3. DISSIPATION

The dissipation of short waves imbedded in a full spectrum poses an outstandingly difficult problem. Here the case of an isolated band of short surface waves in the presence of much longer waves is investigated. The scenario envisioned is a band of strongly generated short waves near $c^{\min}$, in an environment slowly modulated by long waves. Although many wave-wave interactions are possible (including triad interactions; cf. *Valenzuela and Laing* [1972]), these are neglected for simplicity; their inclusion in future works is encouraged.

The mechanism investigated here is an abrupt loss of energy whenever waves exceed some limiting steepness. Two previous arguments concerning a limiting steepness of waves are combined and extended: (1) *Longuet-Higgins* [1969*a*] estimates the fraction of wave energy dissipated per wave cycle, assuming energy in crests exceeding some "critical level" to be lost in that time; (2) *Phillips and Banner* [1974] describe a limiting steepness by requiring that the fluid velocity at the actual surface not exceed the phase speed of the waves. A limiting steepness need not be enforced solely by "breaking"; for example, an abrupt increase in spectral transfer could have a similar effect and could also be modulated by long-wave straining and variations in the drift current. Here the analysis is carried through as if breaking were the sole cause; the precise form of the result should not be taken too seriously.

The first part is a paraphased summary of *Longuet-Higgins* [1969*a*]. Consider a narrow band of short waves, $\omega_1 < \omega < \omega_2$, carrying total wave action A_s:

$$A_s = \int_{\omega_1}^{\omega_2} A'(\omega)\, d\omega \tag{25}$$

The mean square "slope" is

$$s_s{}^2 = \int_{\omega_1}^{\omega_2} S(\omega)\, d\omega \equiv \int_{\omega_1}^{\omega_2} 2(k^3/\omega)A'(\omega)\, d\omega \tag{26}$$

and the mean square frequency is

$$\omega_s{}^2 \equiv s_s{}^{-2} \int_{\omega_1}^{\omega_2} \omega^2 S(\omega)\, d\omega \tag{27}$$

For convenience, a "mean wave number" k_s is defined to relate the total action to mean square slope:

$$k_s{}^3 \equiv \tfrac{1}{2}s_s{}^2\omega_s/A_s \tag{28}$$

This "narrow band" of waves may be thought of as a series of "packets" having frequency ω_s, wave number k_s, and a variable slope-amplitude s which roughly follows a Rayleigh distribution:

$$P(s) = \frac{2s}{s_s{}^2} \exp[-(s/s_s)^2] \tag{29}$$

If all slopes exceeding some critical steepness s^{crit} were reduced to s^{crit}, the fraction of the action so lost would be

$$A^{\text{lost}}/A_s = s_s{}^{-2} \int_{s^{\text{crit}}}^{\infty} [s^2 - (s^{\text{crit}})^2]P(s)\, ds = \exp(-(s^{\text{crit}}/s_s)^2) \tag{30}$$

Assuming that this equals the fraction lost in a single wave cycle, the dissipation rate becomes

$$D^{LH} = A_s(\omega_s/2\pi)e^{-A^c/A} \tag{31}$$

where $s_s{}^2$ is converted to A_s and $(s^{\text{crit}})^2$ to A^c using ω_s and k_s as defined.

In the presence of nonnegligible generation, additional dissipation should be expected, since input to waves already breaking is also wasted. For input apportioned by existing action, an argument like that above indicates that the fraction of the input GA immediately destroyed in breaking waves would again be $\exp(-A^c/A_s)$. Including viscous dissipation as well, the total dissipation takes the form

$$D = [\omega_s/2\pi + G]e^{-A^c/A_s} + 4\nu^m k_s{}^2 \tag{32}$$

where $\nu^m \equiv \mu^m/\rho$ is the molecular kinematic viscosity at the surface. Waves near $c^{\min}$ are strongly generated and so should be "pushed up against the limit" more strongly than longer waves, yet observations of slope spectra show no reliable peak near $c^{\min}$ [e.g., *Plant*, 1982]. Possibly, the stronger generation is countered by a reduction in the maximum allowed (critical) steepness.

What is a reasonable limiting steepness s^{crit}? As described by *Phillips and Banner* [1974], breaking is expected when the actual fluid velocity at the surface matches or exceeds the phase speed of the wave. It is important to include the effects of even a small surface drift as well as variations in phase speed due to apparent gravity, etc. Neglecting viscous (or turbulent) effects and integrating the Bernoulli equation along the actual surface [cf. *Phillips*, 1977], the net velocity $c - u - q$ becomes zero (in a frame moving along with the short-wave phase) just where

$$(g'\zeta - T\nabla^2\zeta)^{\text{crit}} = \tfrac{1}{2}(c - q_s)^2 \tag{33}$$

where q_s is the component of surface fluid velocity parallel to the short-wave progagation direction, at a location where $\zeta \approx \nabla^2\zeta \approx u \approx 0$ (back in the short-wave intrinsic frame). Using the linear measure of steepness as defined in section 2, $s \approx ak$, the result is

$$s^{\text{crit}} \approx \tfrac{1}{2}(1 - q_s/c)^2 \tag{34}$$

Note that ignoring advection momentarily, the maximum effect of q on s^{crit} would occur at $c^{\min}$. Since, however, the shorter waves are advected more than longer ones by the thin drift layer, the maximum effect is shifted slightly toward the longer, gravity-wave side of $c^{\min}$. The surface drift is not necessarily small compared to the short-wave phase speed: For example, $c^{\min} \approx 20$ cm/s $\approx 2\%$ of 10 m/s, which is a fairly typical drift velocity.

How strongly is the effective drift q_s modulated? *Phillips and Banner* [1974] and *Phillips* [1977] neglect readjustment of the drift under the wind, compared to the straining at the

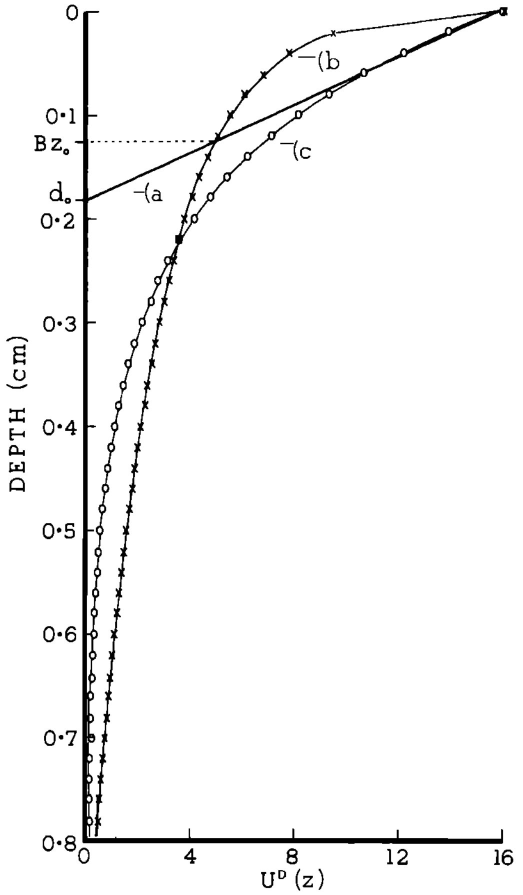

Fig. 3. Model drift profiles: (*a*) laminar, (*b*), logarithmic, and (*c*) exponential (with d_0 reduced to 82%). The depth scale corresponds to centimeters and the velocity scale to centimeters per second for $w_* = 1$ cm/s. The log linear profile formed by joining profiles *a* and *b* at depth Bz_0 corresponds to the "viscous model."

long-wave frequency, and also neglect variations in the applied stress. *Phillips* [1977] gives a compact, exact solution for the resulting surface drift modulation. The pronounced amplification of the drift near the long-wave crests shown there (see especially his Figure 3.10), together with the strongly nonlinear nature of the dissipation term above, suggests the following example:

Consider a limiting case for steep long-waves, where all short-wave dissipation is concentrated at the long-wave crests. Neglecting all variations other than exponential growth, followed by a return to the "base-level" action A_B at each long-wave crest,

$$A(\chi) = A_B\, e^{-(G/\Omega)\chi}, \qquad 0 < \chi < 2\pi, \tag{35}$$

where $\chi \equiv Kx - \Omega t$ is the long-wave phase function. The first harmonic of the modulation A_1 becomes

$$A_1/A_0 \equiv \frac{\displaystyle\int_0^{2\pi} A(\chi)\, e^{-i\chi}\, d\chi}{\displaystyle\int_0^{2\pi} A(\chi)\, d\chi} = \frac{G}{G + i\Omega} \tag{36}$$

For $G \gg \Omega$ the short-wave action becomes concentrated in a spike at the long-wave crests, and $A_1 \rightarrow A_0$ with a phase of 0°. Conversely, for G small in comparison to Ω the short-wave action approaches a "saw-tooth" pattern, and $A_1 \rightarrow GA_0/i\Omega$, with a first harmonic "maximum" 90° ahead of each crest.

4. Surface Drift Evolution

In the short-wave action balance, both U^D and c^{gs} were neglected in comparison to C^L. In the dissipation term, however, U^D appears in relation to c and so need not be small; in fact, as noted above, the surface drift under a 10 m/s wind is roughly equal to the minimum phase speed. A complete description of the time-dependent evolution of the surface drift layer would be an ambitious undertaking; in the following section, an approximate drift model is developed to estimate the effects on short-wave dissipation.

The surface drift U^D is modulated directly by straining and indirectly by induced variations in wind stress (and, possibly, in short-wave dissipation). If the modulation is quick in comparison to the "readjustment time" of the drift layer, the analysis of *Phillips and Banner* [1974] or *Phillips* [1977] may be applied. A measure of this readjustment time is the time required to replace the momentum in the drift layer via the applied stress, $\tau = \rho w_*^2$ (where ρ is the density of the water and w_* is the water friction velocity). For a surface drift of about $16w_*$ [cf. *Wu*, 1975; *Plant and Wright*, 1980], and employing a standard log linear profile (cf. *Tennekes and Lumley*, 1972, pp. 160–161), this time is about 2 s (under a 6-m/s wind, for example). Thus readjustment probably shouldn't be ignored. Also, the surface drift U^D partially advects the short waves. As noted by *Phillips* [1977], a 6-m/s wind generates a viscous sublayer about 2 mm thick, so that for example, this advection is negligible for short waves more than about 10 cm long. In contrast, for waves around 2 cm long (near $c^{\min}$ and also primary scatterers for some radars) the advection would amount to roughly half the surface drift. Ergo, this too should be considered. Finally, the wind stress experienced at the surface will, in general, vary with long-wave phase, which will produce additional variations in the actual and effective drift.

Modeling of the time-dependent drift evolution with long-wave-induced modulations is suggested as a potential avenue of research. For example, work on the modification of the turbulent bottom boundary layer due to wave motion could be used as a starting point [e.g., *Trowbridge and Madsen*, 1984, and references therein]; however, short-wave dissipation (not relevant at the bottom) almost certainly influences the drift. Here, some credibility will be traded for tractability. For example, relaxation is used to model readjustment. Also, in deriving (3), *Stewart and Joy* [1974] assume $\partial U/\partial z \ll \omega$; but for waves near $c^{\min}$, ω is in the range 50–100 s^{-1}, while for a 6-m/s wind the viscous shear $\partial U/\partial z$ approaches 110 s^{-1}. Although the assumption is violated, the results compare favorably in the special case of a purely logarithmic profile to those derived by *Plant and Wright* [1980] with no restriction on the shear (their result is simply $U^a \approx U(0.044\lambda)$).

To evaluate the effective drift $\mathbf{q}$, a model profile for the drift layer must be chosen. To help separate model-dependent from robust results, four models were compared: a purely laminar layer, a purely logarithmic layer, a log linear layer, and an exponential profile,

$$\mathbf{U}^D(z') \approx \mathbf{U}^0 e^{z'/d} \tag{37}$$

where $z' = z - Z$ is the depth below the long-wave surface and $\mathbf{U}^0$ is the drift velocity at the actual surface Z. Since the exponential profile, with a surface value of around $16w_*$, resembles the standard log linear profile (see Figure 3) yet provides the simplest exposition, it is the model shown here. Comparisons with results from a log linear profile and the log profile as employed by *Plant and Wright* [1980] are made in the next section. Also, key results from these two profiles (e.g.,

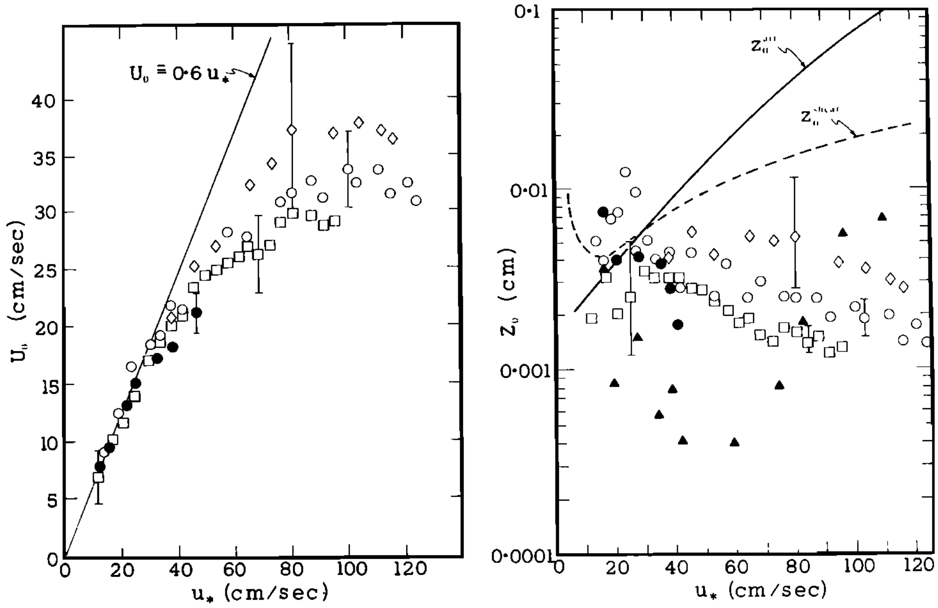

Fig. 4. (Left) Surface drift derived from floats (closed circles), and from short-fetch phase speed data assuming $z_0 = z_0^{air}$: open circles, 36-cm waves; open diamonds 16.5-cm waves; open squares 9.8-cm waves. The line corresponds to $U_0 = 0.60\ u_*$. (Right) Roughness length in water derived from the same data assuming $U_0 = 0.60u_*$. Open points are from *Plant and Wright* [1980], solid points are from Wu (as quoted in *Plant and Wright* [1980]). The open points are as above; solid circles, floats; solid triangles, fixed probe. The solid curve shows z_0^{air}; the dashed curve shows z_0 from the "shear model," for comparison. The upturn of the dashed line at low winds represents the "viscous limit"; i.e., the roughness length is not allowed to fall below the value for a smooth wall (appropriate to the viscous model). (Reprinted, except for the dashed line, from *Plant and Wright* [1980]).

effective drift q and total drift momentum M) are described in the appendices.

The exponential profile yields an effective surface drift (from (3)) of

$$\mathbf{q} \approx \frac{\mathbf{U}^0}{1 + 2kd} \tag{38}$$

Straining

To begin, the effects of long-wave orbital straining on the drift velocity are reviewed, paralleling the arguments of *Longuet-Higgins* [1969b], *Phillips and Banner* [1974], and *Phillips* [1977]. As in these works, the drift shear $\mathbf{v} \equiv \partial \mathbf{U}^D/\partial z$ is assumed to dominate the vertical shear, the long-wave straining $\nabla_H \cdot \mathbf{U}^L = \partial U^L/\partial x$ is assumed to dominate among the horizontal divergence terms, and the drift layer is assumed to be thin compared to K^{-1} (so that U^L is effectively uniform through the depth of the drift layer). Under these assumptions, the drift profile is subjected to nearly uniform vertical stretching by the long-wave strain, so the depth scale d behaves roughly according to

$$D_t d \approx -d(\nabla_H \cdot \mathbf{U}^L) \tag{39}$$

where D_t is the (horizontal) material derivative. In addition (as noted by *Longuet-Higgins* [1969b]), the long-wave straining $\partial U^L/\partial x$ performs vortex stretching on the y component of the vertical shear, $v_y \equiv \partial U_y^D/\partial z$, but not on the x component, $v_x \equiv \partial U_x^D/\partial z$. Vertical differentiation of the horizontal momentum equation yields (with the noted assumptions)

$$D_t\mathbf{v} \approx \mathbf{v}(\nabla_H \mathbf{U}^L) - (\mathbf{v} \cdot \nabla_H)\mathbf{U}^L \tag{40}$$

The surface drift $\mathbf{U}^0$ is proportional to $\mathbf{v}d$, where $\mathbf{v}$ is a suitable shear scale, say, the shear at the surface. Combining (39) and (40), the surface drift is

$$D_t\mathbf{U}^0 \approx -(\mathbf{U}^0 \cdot \nabla_H)\mathbf{U}^L \tag{41}$$

Only the component of $\mathbf{U}^0$ parallel to $\mathbf{U}^L$ is modulated; as mentioned in previous works, the modulations of d and $\mathbf{v}$ exactly cancel for the perpendicular (y) component.

To estimate a relaxation time, it is useful to examine the "drift momentum," given by

$$\mathbf{M} \equiv \int_{-\infty}^{z} \rho \mathbf{U}^D(z)\, dz \sim \rho \mathbf{v} d^2 \sim \rho \mathbf{U}^0 d \tag{42}$$

For completeness, the above arguments lead to an equation of the form

$$D_t\mathbf{M} \approx -\mathbf{M}(\nabla_H \cdot \mathbf{U}^L) - (\mathbf{M} \cdot \nabla_H)\mathbf{U}^L \tag{43}$$

These arguments apply to any self-similar drift profile, using suitable scales for the shear $\mathbf{v}$ and depth d.

The above equations can be integrated exactly to yield $\mathbf{U}^D(z')$ as a function of $\mathbf{U}^L$. For the case where $\mathbf{U}^D$ is parallel to the long-wave propagation the results are shown by *Phillips* [1977] in his figure 3.10 (refered to above) for various values of mean drift and long-wave steepness. However, these equations neglect "turbulent readjustment" in comparison to the long-wave time scale Ω. To model this, relaxation of the drift toward an equilibrium value will be introduced.

To maintain simplicity, the long-wave slope expansion is first applied to d, $\mathbf{v}^0$, $\mathbf{U}^0$, etc.; e.g.,

$$\begin{aligned} d &= d_0 + \varepsilon d_1 e^{i\chi} + \cdots \\ \mathbf{U}^0 &= \mathbf{U}_0{}^0 + \varepsilon \mathbf{U}_1{}^0 e^{i\chi} + \cdots \text{ etc.} \end{aligned} \tag{44}$$

The zero-order (equilibrium) drift is assigned the value referred to above [*Wu*, 1975; *Plant and Wright*, 1980]:

$$\mathbf{U}_0{}^0 \approx 16\mathbf{w}_* \tag{45}$$

where $\mathbf{w}_*$ is the overall mean friction velocity in the water, $w_* = (\tau_0/\rho)^{1/2}$. the viscous shear stress at the surface gives $\mathbf{v}_0 = \tau_0/\mu$, where μ is the effective viscosity at the surface, whence

$$d_0 \approx U_0{}^0/v_0 = 16\nu/w_* \tag{46}$$

where $\nu = \mu/\rho$ is an effective kinematic viscosity at the surface (here, an "eddy viscosity" might be most appropriate). The mean effective drift, using (38) then becomes

$$Q_0 \equiv (\mathbf{q}_0 \cdot \mathbf{k}_0)/\omega_0 = \frac{U_0{}^0 c_0{}^{-1} \cos(\theta_w - \theta_s)}{1 + 2k_0 d_0} \tag{47}$$

Here (and below) the surface shear-stress condition should not be taken too seriously, since the profile is an approximation to a turbulent boundary layer. For example, in the case of a "smooth wall" (i.e., using ν^m) the exponential is a reasonable approximation to a log linear profile, using a value for d_0 reduced to about 82% of the above value (as will be seen in the next section). Conceptually, the shear is matched at some depth within the laminar sublayer rather than at the surface (see Figure 3 again).

This "viscous model" yields a drift momentum $M_0 \approx 256\mu$, which (somewhat surprisingly) is independent of the wind. This is qualitatively true for any self-similar profile where $U_0{}^0$ is proportional to w_* and the depth scale is proportional to $w_*{}^{-1}$ (i.e., for constant ν). The laminar model yields half the above momentum, while the log linear profile yields $M_0 \approx 236\mu$.

In modeling a turbulent boundary layer, the wind dependence of the depth scale (or "roughness length") is a critical consideration. For example, the roughness length in the air ($z_0{}^{\mathrm{air}}$) over water increases rapidly with wind speed (roughly as $w_*{}^2$ see, e.g., Figure 4 (right) [from *Plant and Wright*, 1980]). In their study of the phase speeds of short surface waves, *Plant and Wright* [1980] show two complementary analyses: On one hand, assuming $z_0 \approx z_0{}^{\mathrm{air}}$ results in a "saturation" of drift velocity at high winds (reproduced in Figure 4 (left)); on the other hand, assuming $U^0 \approx 0.6u_*$ results in an estimate of z_0 roughly independent of the wind (as in Figure 4 (right)). Thus in addition to the "viscous model" described above, a "roughness model," with fixed z_0, and a "shear model," where z_0 is proportional to w_* (and hence the surface shear value is fixed), are introduced. The wind dependence of the roughness length in the shear model is intermediate between that of $z_0{}^{\mathrm{air}}$ and a fixed value (see Figure 4 (right) again). A log layer with $z_0 \approx$ .004 cm (a fixed value suggested by Figure 4 (right)) yields $M_0 \approx 1720\rho z_0 w_*$ for $U^0/w_* = 16$. This is exponentially sensitive to the particular value of U^0/w_* chosen, increasing to $2600\rho z_0 w_*$ for $U^0/w_* = 17$. For fixed surface shear, the drift momentum is proportional to τ_0 (i.e., to $w_*{}^2$).

A relaxation of the drift layer toward the equilibrium level $\mathbf{M}_0$ is now introduced. Conceptually, the two terms $\tau - R^D\mathbf{M}$ are added to the momentum balance, (43). The zero-order balance (equilibrium) is then just between these two terms, yielding an estimate of the relaxation rate R^D:

$$R^D \equiv \tau_0/M_0 = \nu/d_0{}^2 \tag{48}$$

For the viscous model, the response time $(R^D)^{-1}$ of the drift decreases with wind as $w_*{}^{-2}$; for the roughness model it decreases as w_*^{-1}; and for the shear model it is fixed. Among the different profiles and depth-scaling models, there is a fair range of values possible, but $(R^D)^{-1}$ generally falls between about 2 and 20 s (for winds from 5 to 15 m/s or so).

At $O(\varepsilon)$, the equations for d, U^0, M, etc. may all self-consistently be given the same relaxation rate; for example,

$$D_t d \approx -d(\nabla_H \cdot \mathbf{U}^L) - R^D(d - d_0) \tag{49}$$

Substituting (44) into (49) and gathering the $O(\varepsilon)$ terms yields

$$d_1 \approx \frac{d_0}{1 + iR^D/\Omega} \tag{50}$$

and (similarly)

$$\mathbf{U}_1{}^0 \approx U_0{}^0\left(\frac{\cos\theta_w}{1 + iR^D/\Omega}, 0\right) \tag{51}$$

where θ_w is the angle between the mean drift and the long-wave propagation direction ($+x$). Defining $Q \equiv (q \cdot k)/\omega$, as implied in (47) and expanding in ε as usual, the $O(\varepsilon)$ effective parallel drift is $Q_1 = Q_1{}^D + Q_1{}^k + Q_1{}^g$, where

$$Q_1{}^q = \frac{Q_0}{1 + iR^D/\Omega}\left(\frac{\cos\theta_s \cos\theta_w}{\cos(\theta_w - \theta_s)} - \frac{2k_0 d_0}{1 + 2k_0 d_0}\right) \tag{52}$$

$$Q_1{}^k = Q_0\left(\frac{\cos\theta_s \cos\theta_w}{\cos(\theta_w - \theta_s)} - \frac{c_0{}^{gs}}{c_0}\cos^2\theta_s - \frac{2k_0 d_0}{1 + 2k_0 d_0}\cos^2\theta_s\right) \tag{53}$$

$$Q_1{}^g = \tfrac{1}{2} g k_0 \omega^{-2} Q_0 \tag{54}$$

In (52) the first term represents the changes in actual surface drift parallel to $\mathbf{k}$; the second term represents the effect of changes in the drift depth scale d on the advection rate of the short waves. In (53) the first two terms represent the changes in phase speed of the short waves (one via $\mathbf{k}$, two via ω), and the third term represents the change in advection rate due to varying the depth scale k of the short waves. Finally, (54) represents the change in short-wave phase speed (via ω) due to vertical acceleration by the long waves.

Variable Stress

The response to a variable surface stress is treated separately to allow downward shear propagation. The same sort of "relaxed approach" is taken to derive an $O(\varepsilon)$ solution to the stress variations. First, recall the expansion of the varying stress in terms of long-wave harmonics:

$$\tau = \tau_0 \,\mathrm{Re}\,[1 + \varepsilon t_1 e^{i\chi} + \cdots] \tag{20}$$

(where, as mentioned in section 2, t_1 may be anything from 0 to 20). Now allow the harmonic response to have a complex depth dependence:

$$\mathbf{U}'(z') = \mathrm{Re}\,[\varepsilon e^{i\chi}\mathbf{U}_1'(z') + \varepsilon^2 e^{i2\chi}\mathbf{U}_2'(z') + \cdots] \tag{55}$$

The $O(\varepsilon)$ viscous stress equation is assumed to "relax" at the same rate R^D as above, so that (for constant ν)

$$\mathbf{U}_1' D_t e^{i\chi} = \left(\nu \frac{\partial^2 \mathbf{U}_1'}{\partial z^2} - R^D\,\mathbf{U}_1'\right)e^{i\chi} \tag{56}$$

Assuming an exponential form for $\mathbf{U}_1'(z)$ yields a complex depth scale:

$$d_1' = \left(\frac{\nu}{R^D - i\Omega}\right)^{1/2} = \frac{d_0}{(1 - i\Omega/R^D)^{1/2}} \tag{57}$$

(where the second equality holds provided d_0 and R^D are related as in (48)).

For a surface boundary condition of the form $\partial U/\partial z \sim t_1 v_0$ (i.e., demanding that the surface shear is in phase with the surface stress),

$$\mathbf{U}_1'(z') \sim \frac{U_0{}^0\, e^{z'/d'}}{(1 - i\Omega/R^D)^{1/2}} \tag{58}$$

(since $U_0{}^0 \equiv d_0 v_0$). If $U(0)$ is to remain proportional to w_* as $\Omega \to 0$, then (since $w_* = (\rho^{-1}\tau_0)^{1/2}$) the constant of proportionality in (58) must be $\frac{1}{2}t_1$ (at first order), or half the value given by a shear condition with viscosity independent of wind. Substituting this into (3), subtracting, and dividing by the short-wave phase speed, the net modulation of the effective drift by the stress is

$$Q_1{}^\tau = \tfrac{1}{2}t_1\left(\frac{U_0{}^0 c_0{}^{-1} \cos(\theta_w - \theta_s)}{(1 - i\Omega/R^D)^{1/2} + 2k_0 d_0}\right) \tag{59}$$

The above assumes constant ν. In the viscous model, about $11w_*$ of the total $16w_*$ surface drift is accounted for in the laminar sublayer; in this case, the above is not unreasonable (e.g., using the "reduced d_0"). In the roughness or shear model, the drift layer becomes more turbulent as the wind increases, and the laminar sublayer is reduced and finally disappears. The relation between the complex exponential and log linear profiles (for example) is then less clear. To make use of this "varying stress" solution, an "equivalent depth" $(2kd)^e$ is introduced for the alternate profiles. In (59) the scaled depth $2kd$ helps determine the phase of the modulation, as it affects the short waves. It is therefore appropriate to consider the equivalent depth as a time scaling, amenable to a treatment similar to that of the relaxation rate R^D. Define first an "advection depth" z^a, at which the actual drift velocity equals the advection velocity of the short-waves; then choose $(2kd)^e$ to preserve the ratio of the momentum M^a, contained in the drift layer above z^a, to the total drift momentum M_0. For the exponential profile, M^a is simply

$$M^a = \int_{-z^a}^{0} \rho U_0 e^{z/d}\, dz = \frac{M_0}{1 + 2k_0 d_0} \tag{60}$$

Given M^a and M_0 from another profile (e.g., from Appendix B), the equivalent depth for use in (59) is then simply

$$(2kd)^e = M_0/M^a - 1 \tag{61}$$

5. APPLICATION

We now return to the short-wave model discussed near the end of section two. The zero-order balance provides the mean level of short-wave action, A_0, for given wind conditions:

$$A_0 = A_0{}^c\left(\ln\left[\frac{G_0 + \omega_0/2\pi}{G_0 - 4\nu k_0{}^2}\right]\right)^{-1} \tag{62}$$

The short-wave relaxation rate R^A is

$$R^A = \frac{A_0{}^c}{A_0}(G_0 - 4\nu k_0{}^2) \tag{63}$$

Which is generally greater than the short-wave growth rate G. For "peak frequency" waves, *Longuet-Higgins* [1969*a*] found a "saturation ratio" $A_0{}^c/A_0$ of the order of 10. Here the rather strong wind forcing near $c^{\min}$ drives this ratio down to about 2 for moderately strong winds, yielding relaxation rates in rough agreement with those of *Keller and Wright* [1975] and *Valenzuela and Wright* [1979].

The net forcing F^A is now separated into parts owing to (1) straining of the drift (F^q), (2) the varying wind stress (F^τ), (3) the apparent gravity (F^g), and (4) short-wave number changes (F^k):

$$F^A = F^q + F^\tau + F^g + F^k \tag{64}$$

where

$$F^q = -R^A\left(\frac{4Q_1{}^q}{1 - Q_0}\right) \tag{65}$$

$$F^\tau = G_1{}^\tau(1 - e^{-A_0{}^c/A_0}) - R^A\left(\frac{4Q_1{}^\tau}{1 - Q_0}\right) \tag{66}$$

$$F^g = G_1{}^g(1 - e^{-A_0{}^c/A_0}) - R^A\left(\frac{4Q_1{}^g}{1 - Q_0} + \tfrac{1}{2}gk_0\omega_0{}^{-2}\right) + (\tfrac{1}{2}gk_0\omega_0{}^{-2})(\omega_0/2\pi)e^{-A_0{}^c/A_0} \tag{67}$$

$$F^k = G_1{}^k(1 - e^{-A_0{}^c/A_0}) - R^A\left(\frac{4Q_1^k}{1 - Q_0} + (3 - c_0{}^{gs}/c_0)\cos^2\theta_s\right) - ((c_0{}^{gs}/c_0)(\omega/2\pi)e^{-A_0{}^c/A_0} + 8\nu k_0{}^2)\cos^2\theta_s \tag{68}$$

Here the terms multiplied by R^A all represent forcing due to changes in the critical steepness criterion. The "Q terms" derive from changes in the effective drift, already identified with the four basic sources in (52), (53), (54), and (59). The other "R^A term" in (67) is due to the change in short-wave orbital velocity at fixed k induced by vertical acceleration; the remaining R^A term, in (68) derives from the change in short-wave orbital velocity associated with changes in k. The "G terms" represent the net forcing due to changes in input from the wind, associated with three of the four basic sources; recall that the fraction $\exp(-A_0c/A_0)$ is directed at breaking waves, which cannot accept more action. The last term of (67) accounts for a change in the time period during which the breaking occurs, i.e., the change in $2\pi/\omega$ induced by vertical acceleration. The similar term in (68) arises from the change in $2\pi/\omega$ due to changes in k. Finally, the last term of (68) is the change in viscous dissipation for a change in k.

The forcing term F^k represents the net imbalance arising from changes in the wavelength of the short waves: As the packet is squeezed (for example), the wave number increases, moving the equilibrium action level down along the slope of the "equilibrium spectrum." Since the detected wave number (e.g., by radar) is not likely to vary in the same way as the packet wave number, it is sensible to translate this shift in wave number to an apparent shift in action at a fixed wave number:

$$\frac{\partial A^k}{\partial \chi} = \frac{\partial k_x}{\partial \chi}\frac{\partial A}{\partial k_x} \tag{69}$$

The action spectrum is used to evaluate this "Boltzmann transport," since these wave number changes are dynamically induced, and action is conserved as the short-wave number changes.

Spectral Comparison

The zero-order balance implied by the above model is now compared to observations of high wave number slopes to see whether the spectral slope (and hence transport) may also be predicted from this model. Although in reality the waves are imbedded in a continuous spectrum, the model developed above considers an isolated band of short waves under the influence of a much longer wave train. The steepness of the short waves clearly depends on the bandwidth chosen from a continuous spectrum. Thus it is appropriate to ask, how can a comparison be made? Appeal is made to the concept of a physical bandwidth; i.e., suppose it is sensible to assign a characteristic coherence length and time to each wavelength. Then the spectrum of short waves can be viewed in physical space as an agglomeration of many wave packets, each having different central wave number and frequency, and each having finite extent in space and time. The presumptions required then amout to: (1) each packet is large enough to be detected near its central wave number, and (2) other nonlinear interactions are negligible compared to either the long-wave forcing

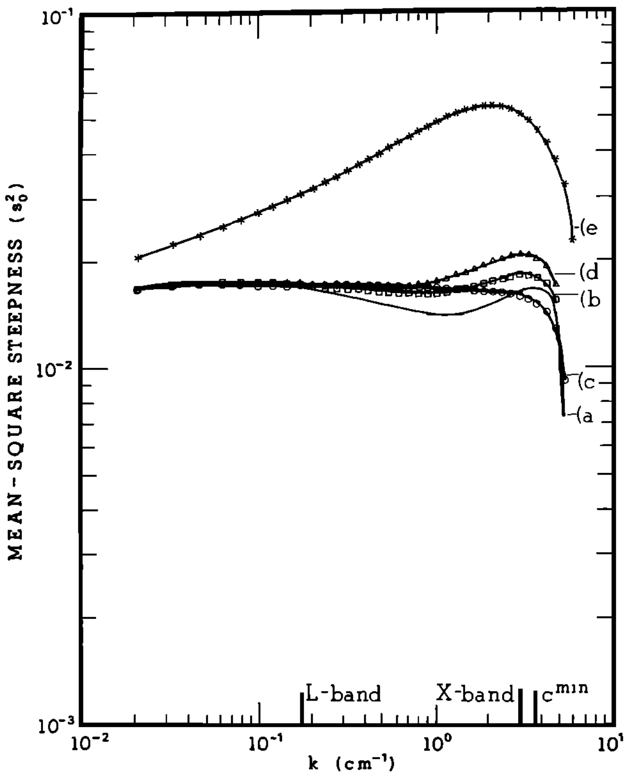

Fig. 5. Model spectra for $u_* = 20$ cm/s: (*a*) laminar drift (plain curve), (*b*) log linear profile (circles), (*c*) logarithmic (triangles), (*d*) exponential (crosses), and (*e*) with no drift (diamonds). Marks show location of 35-cm (L band), 2-cm (X band), and 1.7-cm (c^{min}) short waves.

or the dissipative balance (e.g., encounters between packets are either rare enough or weak enough in their effect to be ignored). Given the extremely rapid growth of wave near c^{min} (e.g., *Larson and Wright* [1975] find doubling times of the order of three wave periods near c^{min} under about 8-m/s winds), this neglect of the "other" interactions is not completely unreasonable.

On dimensional grounds, the slope spectrum $S(k)$ should have roughly a k^{-1} dependence (as supported by observations, [e.g., *Plant*, 1982]; say, $S(k) \approx bk^{-1}$. For discussion, suppose each packet looks like a band of wave numbers taken from this mean spectrum. The mean square slope contained in a band $k - \frac{1}{2}\Delta k$ to $k + \frac{1}{2}\Delta k$ (as in (26)) then becomes

$$s_s^2 \approx \int_{k-\Delta k/2}^{k+\Delta k/2} bk^{-1}\,dk \approx 2b\tanh^{-1}(\Delta k/2k) \approx (\Delta k/k)b \qquad \Delta k \ll 2k \tag{70}$$

Measuring the spectral level at wave number k^M (with antenna bandwidth Δk^M) is roughly equivalent to an integration over all packets with central wave numbers k^P ranging from $k^M - \frac{1}{2}\Delta k^P$ to $k^M + \frac{1}{2}\Delta k^P$. From each of these packets, the measurement would detect a fraction $\Delta k^M/\Delta k^P$ of the packet's slope content; hence the result of the measurement simply yields $(\Delta k^M/k^M)b$, independent of Δk^P. The physical slope limitation, however, depends on the physical bandwidth Δk^P. Thus a comparison of spectral shape may be made, most conveniently with wave-number-weighted (or frequency-weighted) slope spectra, $kS(k) \equiv b(k)$, as long as the weighted spectrum $b(k)$ is a weak function of k and provided Δk^P and Δk^M are small compared to $2k$. The comparison of the magnitudes of the measured and predicted values of $b(k)$ depends on the unknown physical bandwidth as well as the degree of saturation.

Since F^k represents the change in $G - D$ due to changes in k (i.e., in k_x), while R^A represents the rate of change of A due to changes in $G - D$, the k_x-dependence of $A = (\rho\omega k^{-3})(\Delta k^P/k)s_0^2$ is given by the model as

$$\partial A/\partial k_x = (-F^k/R^A)(A_0/k_{0x}) \tag{71}$$

Thus if the shape comparison proves acceptable, the model prediction at fixed wave number is simply given by replacing F^k in the above solution by $-i\Omega F^k/R^A$ (where $-i\Omega$ represents the fractional rate of change of k_x due to the long-wave straining). The net "conservative forcing" (combining this "spectral transport" with the straining term $-i\Omega$) is then $F^c = -i\Omega(1 + F^k/R^A)$.

In his investigation of "a relationship between wind stress and waveslope," *Plant* [1982] compares many measurements of high-frequency slope spectra, from both wavetanks and the open ocean and by several methods (including radar backscatter, laser slope-meter, sun glitter, and Cox's refraction method). Although individual data sets produce a variety of results, his overall conclusion apears to be that the upwind-downwind slope spectrum has roughly an f^{-1} frequency dependence over a range from about twice the peak frequency to at least 20 Hz (c^{min} occurs near 11 Hz) and is fairly constant over a wide range of wind speeds. By implication, $b(k, \tau)$ is expected to be approximately constant with wave number (as indicated above).

As the relative growth rate G/ω increases, the average steepness of the waves is pushed closer to the limit s^{crit} until the dissipation balances the input. Thus as mentioned in section 3, were a uniform limit imposed, the peak in G/ω near c^{min}

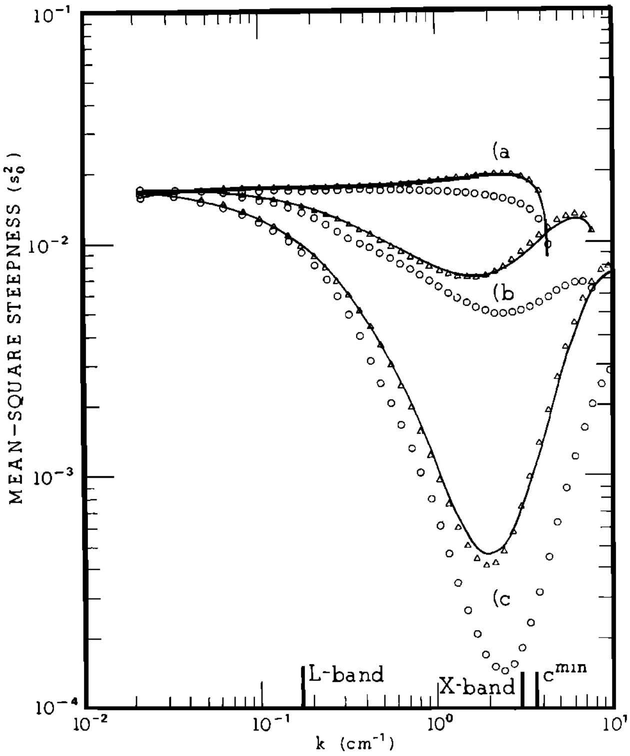

Fig. 6. Spectra for the "viscous model" ($z_0 \sim w_*^{-1}$), using a log linear profile (plain curve), a log profile (circles), and the 82% reduced exponential (triangles). Air friction velocity is $u_* =$ (*a*) 16 cm/s, (*b*) 32 cm/s, and (*c*) 48 cm/s. Marks show location of 35-cm (L band), 2-cm (X band), and 1.7-cm (c^{min}) short waves.

would produce a corresponding peak in the slope spectrum; yet, no such peak is reliably observed. In the dissipation model posed above, the limiting steepness is not uniform; it depends on the ratio of effective surface drift to phase speed. Thus this steepness criterion has a roughly corresponding minimum near the most strongly generated waves. The two effects can virtually cancel over a broad range of wave numbers, yielding model "spectra" $b(k)$ which are nearly flat (see Figure 5). Since each spectral component "samples" the drift to different depths, this "spectral comparison" is a fairly rigorous test of the difference between profiles. As Figure 5 shows, the differneces between results from the four drift profiles are minor (at $u_* = 16$ cm/s) compared to the difference from the model spectrum neglecting drift effects.

The wind speed dependence of radar backscatter allows remote estimation of winds and so is fairly well studied. Although there are uncertainties associated with, for example, atmospheric stability, these studies indicate a wind dependence of radar cross section (associated with rms steepness) ranging from about $U^{1/2}$, for L band backscatter from roughly 35-cm waves, up to about U^2 for X band backscatter from 2-cm Bragg waves [*Thompson et al.*, 1983; *Keller et al.*, 1985, and references therein]. Thus $b(k, \tau)$ is expected to be a weak function of wind at 35-cm wavelengths, becoming more sensitive to τ as the wave number increases toward 2-cm waves. At both points the steepness increases somewhat with wind.

As the model wind speed is increased, the differences due to the different profiles become more pronounced. For the viscous model, the exponential profile can match the effect of the log layer, using a reduced depth scale d_0 of 82% of the value given by (46) (see Figure 6). In this "viscous case" the purely logarithmic approximation performs relatively poorly, overestimating severely the effective drift at high wave numbers (Figure 6 again). For the modulation evaluation (where use of the log linear profile would be cumbersome) the "reduced exponential" is therefore chosen. In the "roughness" and "shear" models, the fraction of the drift velocity accounted for by the laminar sublayer varies with windspeed; thus no uniform "reduction" of d_0 applies. In these two cases the log profile is a better approximation (see Figures 7 and 8) and will be used for the modulation analysis (the momenta M_0 and M^a for use in (61) are given in Appendix B).

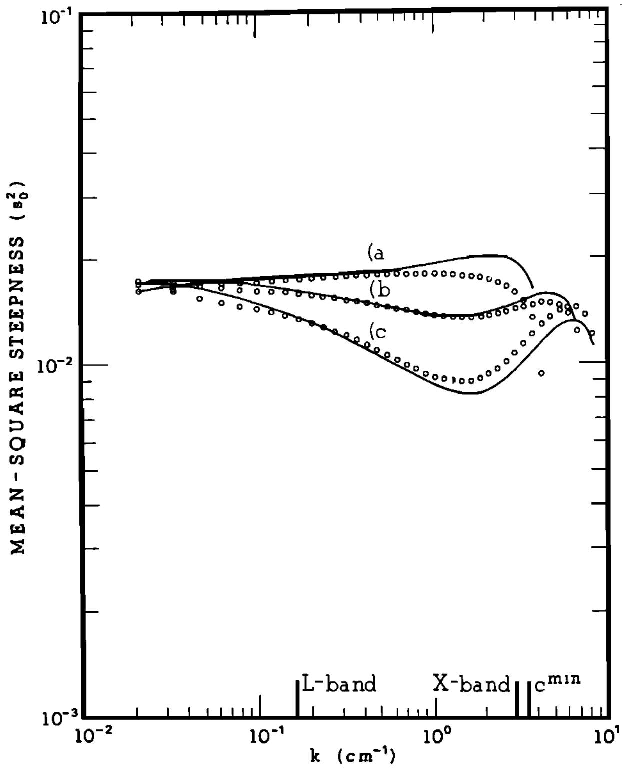

Fig. 8. Spectra for the "shear model" ($z_0 \sim w_*$), using a log linear profile (plain curve) or a log profile (circles). Air friction velocity is $u_* =$ (*a*) 16 cm/s, (*b*) 32 cm/s, and (*c*) 48 cm/s. Marks show location of 35-cm (L band), 2-cm (X band), and 1.7-cm (c^{min}) short waves.

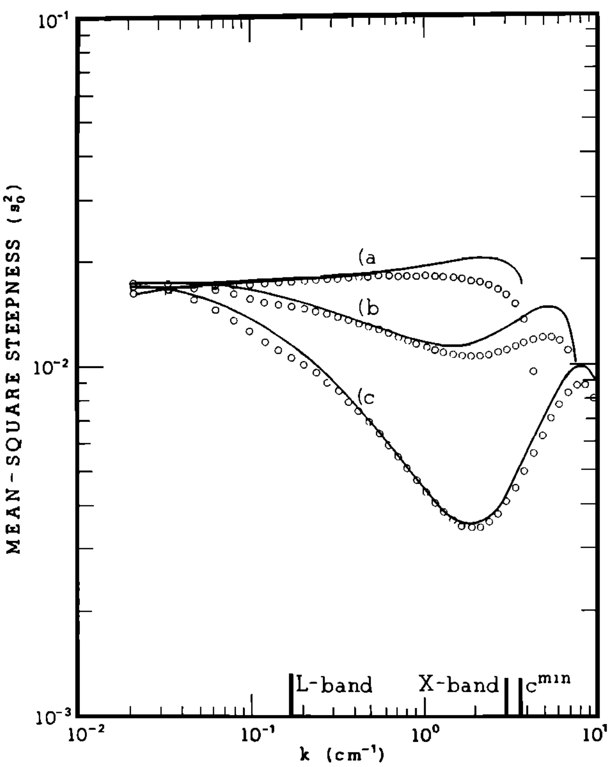

Fig. 7. Spectra for the "roughness model" ($z_0 \approx .004$ cm), using a log linear profile (plain curve) or a log profile (circles). Air friction velocity is $u_* =$ (*a*) 16 cm/s, (*b*) 32 cm/s, and (*c*) 48 cm/s. Marks show location of 35-cm (L band), 2-cm (X band), and 1.7-cm (c^{min}) short waves.

Among the different models for depth scale versus wind (Figure 6 to 8) the shear model yields spectral levels having the least variation with wave number overall, in best accord with the above observations. All three models show a decrease in steepness with wind, contrary to the observations; however, the decrease shown in the shear model is not as severe, again in best accord. A stronger wind dependence (e.g., $z_0 \approx z_0^{\text{air}} \sim w_*^2$; not shown) performs better by this wind-dependence criterion. As caveats, the magnitudes of the model levels are somewhat high (requiring "physical bandwidths" comparable to wave number to match absolute magnitudes); also, no "overshoot effect" is predicted.

SHORT-WAVE MODULATIONS

The models are now compared with some recent observations, described by *Plant et al.* [1983]. In the cases chosen for comparison, the wind is roughly aligned with both long- and short-wave propagation directions (i.e., $\theta_s = \theta_w = 0°$). The two "short" wavelengths chosen for comparison are 2.1 cm, corresponding to the X band (9.3 GHz) radar directed downward 40° from horizontal, and 12 cm, corresponding to the L band (1.5 GHz) at 30° depression angle (as in *Plant et al.* [1983]; in

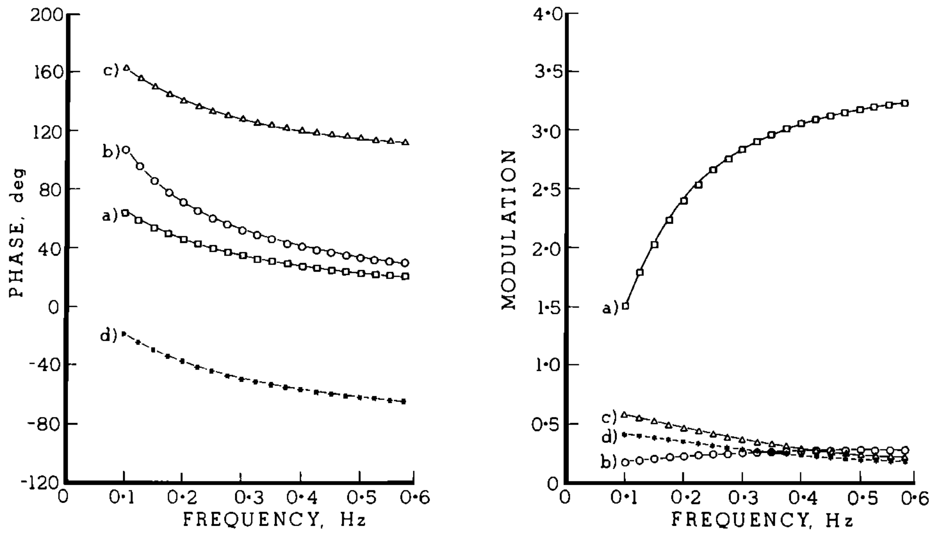

Fig. 9. (Left) Phase ϕ and (right) magnitude $|m|$ of modulations of 2.1-cm waves, due to (*a*) "direct forcing" (squares), (*b*) changes in apparent gravity (circles), (*c*) straining of the drift (triangles), and (*d*) modulated stress (crosses). Results shown are for $z_0 = .004$ cm and $u_* = 16$ cm/s; the stress modulation factor t_1 is 1.

both cases, their vertical polarization data is shown for the comparison).

For the model calculations the physical constants used are $g = 980$ cm/s^2, $T = 72$ cm^2/s, $\rho = 1.026$ g/cm^3, and $\nu^m = 0.012$ cm^2/s. For example, under a 7- to 8-m/s wind, (19) yields short-wave growth rates of about 1.9 s^{-1} for the 2.1-cm waves and about 0.30-s^{-1} for the 12-cm waves (or *e*-folding times of about six and 13 short-wave periods, respectively). The relaxation rates R^4, from (63), are about 3.3 s^{-1} for the 2.1-cm waves, and .75 s^{-1} for the 12-cm waves, or about 1.7 and 2.5 times the respective growth rates (comparable to the value of 2 times the growth rate, as found by *Keller and Wright* [1975], for their first-order relaxation model).

Measured short-wave modulations per unit long-wave steepness (or modulation transfer functions) are reproduced from *Plant et al.* [1983] for both the 2.1- (Figure 1) and 12-cm (Figure 2) short waves. For the range of conditions observed, these MTFs range roughly from 3 to 12 and generally decrease with increasing long-wave frequency. The 2.1-cm MTFs also decrease with increasing wind, while the 12-cm MTFs are insensitive. The phases of the 2.1-cm MTFs fall in the range 0 to 30° ahead of the long waves (i.e., maximum short-wave amplitudes just ahead of long-wave crests) and are independent of the long-wave frequency. The 12-cm MTFs decrease in phase from about 20° ahead of 8-s long waves to slightly behind 3-s waves. For comparison, the optical measurements of *Monaldo and Kasevich* [1982], taken under 5-m/s winds, indicate a constant MTF of about 9, leading by 90°, regardless of short-wavelength or long-wave frequency (for 3-, 11.5-, and 30-cm short waves on long waves with periods between 3 and 8 s). Since, as mentioned in the introduction, the optical long-wave slope measurements appear slightly less reliable than the Doppler velocities, comparison here will favor the radar results.

The model predictions for 2.1-cm waves under gentle winds ($u_* = 16$ cm/s, corresponding to about a 4-m/s wind) are first shown broken down into the phases and magnitudes of the modulations due to "conservative forcing" $F^c(\equiv -i\Omega(1 + F^k/$

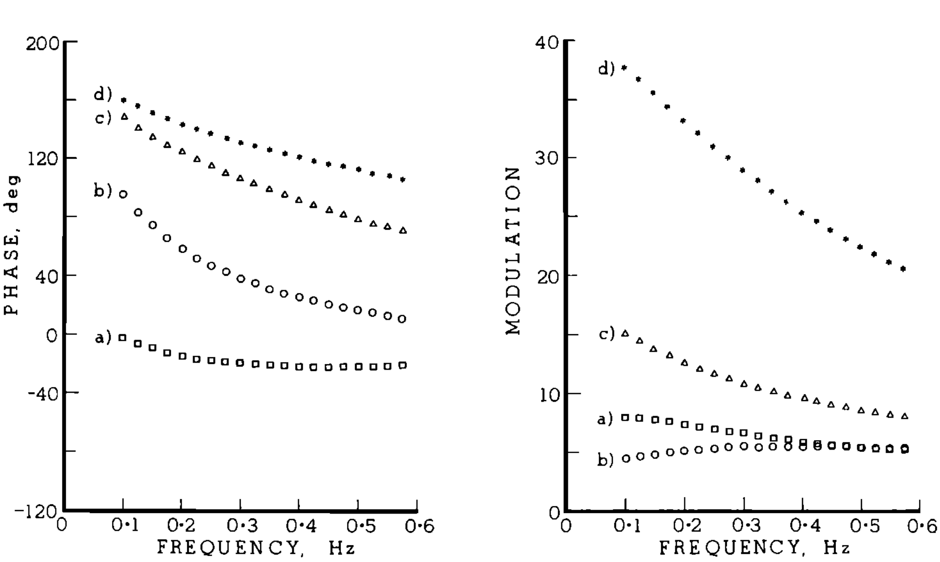

Fig. 10. Net modulations of 2.1-cm waves, with stress modulation $t_1 = 20$; viscous model ($z_0 \sim w_*^{-1}$). For $u_* = (a)$ 16, (*b*) 24, (*c*) 32, and (*d*) 40 cm/s (corresponding roughly to 4-, 6-, 8-, and 10-m/s wind at 10 m).

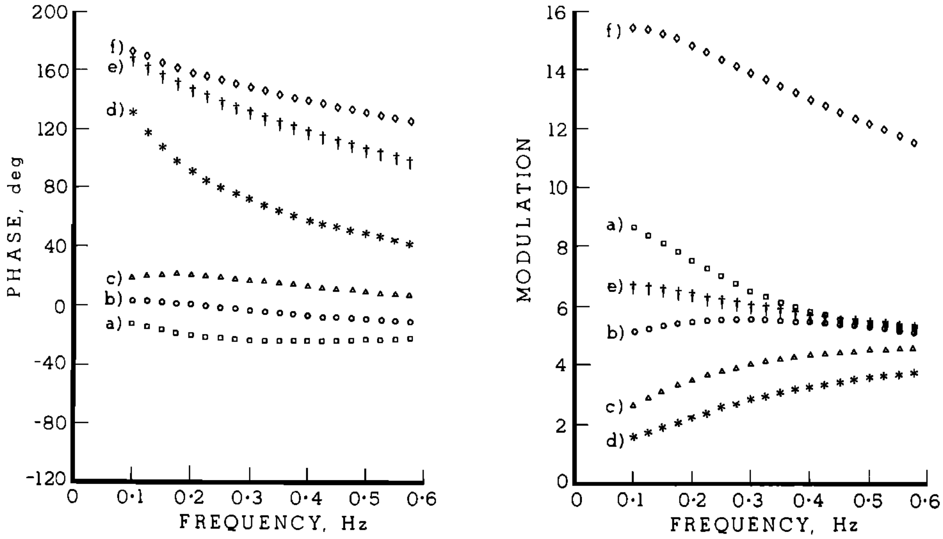

Fig. 11. Net modulations of 2.1-cm waves, with stress modulations $t_1 = 20$; roughness model ($z_0 = 0.004$ cm). For $u_* =$ (*a*) 16, (*b*) 24, (*c*) 32, (*d*) 40, (*e*) 48, and (*f*) 56 cm/sec (corresponding roughly to 4-, 6-, 8-, 10-, 12-, and 14-m/s wind at 10 m).

R^4)), apparent gravity F^g, drift modulation F^q, and the modulated stress F^τ (Figure 9). For both the 2.1- and 12-cm waves, the direct forcing terms effect a modulation increasing in magnitude with Ω. Although the overall magnitude can be altered by (for example) assuming a different spectral slope, the increase with long-wave frequency is an unavoidable consequence of the balance between forcing at a rate dependent on Ω against relaxation at a fixed rate R^4. The forcing due to changes in apparent gravity has the wrong phase; apparently, the enhancement of dissipation near the long-wave crests (due mostly to slowing the phase speed) overwhelms the increase in amplitude at fixed action under reduced gravity (included in the figure calculations, although it does not enter as an action-forcing term in (67)). The forcing due to modulation of the mean drift by straining yields a somewhat stronger effect and decreases in magnitude with long-wave frequency, but the phase is again almost exactly reversed (i.e., maximum amplitudes are induced in the trough). Finally, the net effect of a modulated stress has both the right trend with long-wave frequency and about the right phase. Maximum growth at the crests would by itself induce maximum amplitudes on the rear faces (as noted in the introduction); however, the varying stress also induces maximum drift on the rear faces, and hence maximum dissipation there, largely opposing the effect of growth and resulting in a net maximum of reduced size near the crests. The curves shown in Figure 9 correspond to $t_1 = 1$; in order to produce modulations resembling the measurements, keeping the rest of the model as is, requires a stress modulation much greater than this. In the absence of any firm knowledge regarding its magnitude (or phase) we are more or less free to speculate; thus for comparison, the model results shown below use $t_1 = 20$. Although this is rather large, it may not be unreasonable; for example, in his "rapid distortion" model, *Townsend* [1980] calculates shear stress modulations of the order of 15 to 20 times the long-wave steepness, with maxima near the crests (see also the discussion, below).

Next, consider the wind dependence. As mentioned, the radar observations of 2.1-cm waves (Figure 1) show a decrease

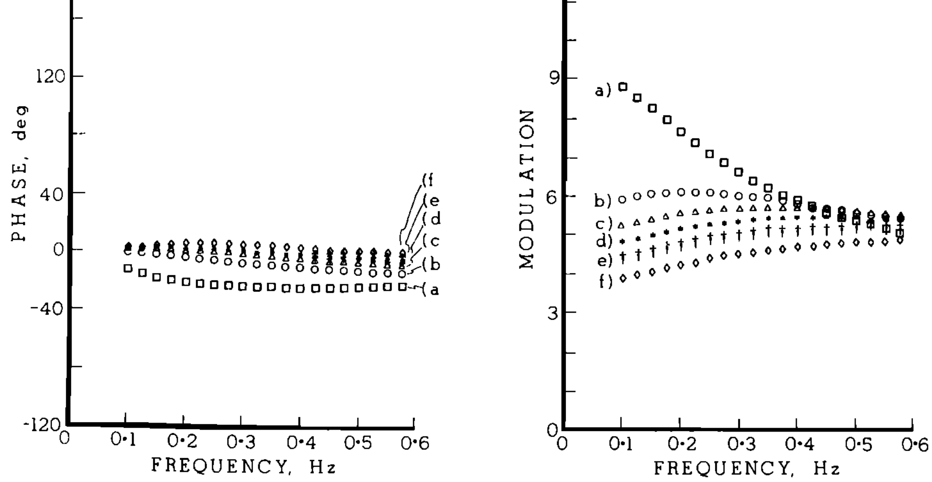

Fig. 12. Net modulations of 2.1-cm waves, with stress modulation $t_1 = 20$; shear model ($z_0 \sim w_*$). For u_* as in Figure 11.

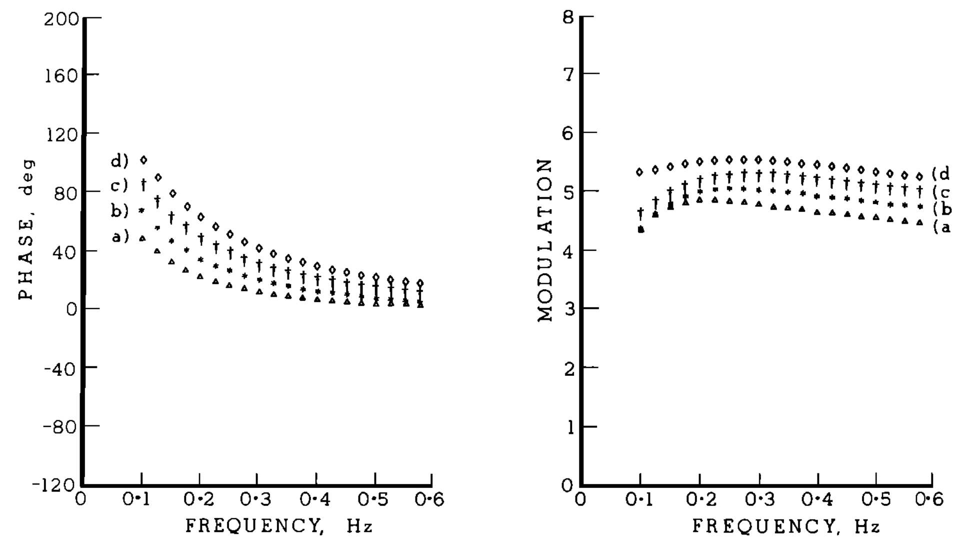

Fig. 13. Net modulations of 12-cm waves, with stress modulation $t_1 = 20$; shear model ($z_0 \sim w_*$). For $u_* =$ (*a*) 32, (*b*) 40, (*c*) 48, and (*d*) 56 cm/s (corresponding roughly to 8-, 10-, 12-, and 14-m/s wind at 10 m).

in modulation with increasing wind (over the range 5 to 14 m/s), while the 12-cm modulations (Figure 2) are insensitive to windspeed (over the range 7 to 15 m/s). The net model predictions corresponding to the three different drift-scaling models ("viscous," "roughness," and "shear") are shown in Figures 10 to 12. These modulations are mostly due to the varying stress ($t_1 = 20$). The "shear model" again produces results most nearly resembling the observations, both in terms of decreasing magnitude with wind and nearly fixed phase. The shear model results (only) are also shown for the 12-cm short waves (Figure 13). Although the overall match is far from perfect (particularly the trend in phase with short wavelength), it is good enough to be encouraging.

The performance of the model depends on both the wind dependence of z_0 and its absolute magnitude. The (best) results of the "shear model," (Figures 12 and 13) correspond to a roughness length matching the viscous solution at about $u_* =$ 16 cm/s and increasing as w_* increases (again, a model with $z_0 \sim w_*^2$ also performs well). With a smaller absolute value (for example), the decrease with wind is less rapid, or even reversed. Also, the phase of the response varies, owing to the different relaxation rates of the drift layer for different values of z_0. The changes in the model behavior with the magnitude of z_0 are significant; e.g., a 10% change renders the results completely different from the observations. These results therefore represent a model in which the response of the drift is "tuned" to match that of the waves, especially with respect to timing. Such a "tuned response" is probably not coincidence; rather (if this tuning exists), the evolution of the drift and short waves must be coupled.

Clearly, it is unlikely that a physically based model would have produced accurate predictions beforehand; there are simply too many ill-known factors. Instead, the observations are used as a guide by which to select from these factors those most likely to be important.

6. DISCUSSION

Several observations have contraindicated the use of drift-enhanced dissipation to explain the behavior of short surface waves. For example, the advection velocities measured by *Plant and Wright* [1980] are independent of fetch. Also, the spectral levels observed are nearly independent of the wind, whereas (as pointed out by *Plant and Wright* [1977]) a drift current proportional to w_* was expected to reduce the observed levels with increasing wind by quite noticeable amounts.

Conversely, a superficial examination of the effect of a modulated drift (cf. the example in section 3) indicated an easy way to account for the tendency of short-wave maxima to occur forward of long-wave crests.

Ironically, according to the analysis presented here, all three of the above have proven misleading. The response time of the drift is of the same order as that of the short waves; hence, no fetch dependence. The increase in dissipation can balance the increase in direct input from the wind; hence, spectral levels can be nearly independent of the wind. Finally, for small modulations, the enhancement of dissipation alone near long-wave crests would result in short-wave maxima near the troughs, rather than crests. It is the combination of dissipation and growth under varying stress that appears to produce the correct phase.

In the above, rather large stress variations (of the order of 20 times the long-wave slope) were invoked to help account for the observed short-wave modulations. The reason such a large value is needed is that the resulting modulations of growth and dissipation almost directly oppose one another (shifted only by the response time of the drift). If, for example, the phase of the drift were delayed further, the magnitude of the response would increase; a corresponding shift forward of the stress maximum could maintain the phase of the amplitude maximum. Reexamination of the drift development and the stress modulation could reduce the "implied" magnitude of t_1 significantly.

An upper bound on the stress modulation is indirectly available. In their application of the first-order relaxation model, *Keller and Wright* [1975] show the modulation magnitude versus long-wave steepness "ε" (reproduced as Figure 14). This modulation "saturates" at long-wave steepness of the order of .05 to .07, implying that no component of modulation can exceed about 15 to 20 times the steepness (e.g., if the minimum stress $\tau_0(1 - t_1\varepsilon)$ is to remain nonnegative). Conversely, a stress modulation t_1 of the order of 15 to 20 would explain the saturation. Again, a value of the order of 15–20 is in rough agreement with the shear stress variations in *Town-*

where κ is Von Karman's constant (assigned the value 0.40) and the matching point Bz_0 is defined by requiring a single velocity value at the interface between the laminar and logarithmic sublayers:

$$V_0 \equiv \left(\frac{w_*^2}{v^m}\right)Bz_0 \equiv \frac{w_*}{\kappa} \ln(1+B) \tag{A2}$$

One possible solution for B is 0 (always); however, it is the larger solution (when it exists) which is of interest. By comparing the projected logarithmic shear at the surface to the viscous shear, it is found that such a positive solution exists whenever $z_0 < v^m/\kappa w_*$; for greater "roughness," no laminar sublayer exists. In the case of a smooth wall the above should reduce approximately to a "standard" model [e.g., *Tennekes and Lumley*, 1972, pp. 160–161]. Thus the "viscous roughness" z_0^v is defined as

$$z_0^v \equiv v^m/w_* e^2 \tag{A3}$$

so that $\kappa^{-1} \ln(z/z_0^v) \simeq 5 + \kappa^{-1}\ln(zw_*/v^m)$. With this value, the "matching velocity" V_0 is about $11w_*$, so that most of the drift velocity is attained in the viscous sublayer.

The thickness Dz_0 of the boundary layer is established by the surface drift value U_0:

$$U_0 = \frac{w_*}{\kappa}\ln(1+D)$$

or

$$D \equiv e^{\kappa U_0/w_*} - 1 \tag{A4}$$

The effective surface drift q is to be found from (3):

$$\begin{aligned} q &= 2k\int_0^{Bz_0} (w_*^2/v^m) z e^{-2kz}\,dz + 2k\int_{Dz_0}^{\infty} U_0 e^{-2kz}\,dz \\ &\quad + 2k\int_{Bz_0}^{Dz_0} (w_*/\kappa)\ln(1+z/z_0) e^{-2kz}\,dz \\ &= \frac{w_*^2}{2kv}(1 - e^{-\alpha B} - \alpha B e^{-\alpha B}) + U_0 e^{-\alpha D} \\ &\quad + \frac{w_* e^{\alpha}}{\kappa}\left([-e^{-\alpha t}\ln t]_{1+B}^{1+D} + \int_{1+B}^{1+D} t^{-1}e^{-\alpha t}\,dt\right) \\ &= \frac{w_*^2}{2kv^m}(1-e^{-\alpha B}) + \frac{w_* e^{\alpha}}{\kappa}(E_1(\alpha(1+B)) - E_1(\alpha(1+D))) \end{aligned} \tag{A5}$$

where $\alpha \equiv 2kz_0$, $t \equiv 1 + z/z_0$, and $E_1(x)$ is the "exponential integral function," evaluated via the series [*Abramowitz and Stegun*, 1965, p. 229]

$$E_1(x) = -\gamma - \ln x - \sum_{n=1}^{\infty} \frac{(-x)^n}{nn!} \tag{A6}$$

where $\gamma = .57721 \cdots$ is Euler's constant.

Finally, the total drift momentum is

$$\begin{aligned} M_0 &\equiv \int_0^{Bz_0} [U_0 - z(w_*^2/v^m)]\,dz \\ &\quad + \int_{Bz_0}^{Dz_0}\left[U_0 - \frac{w_*}{\kappa}\ln(1+z/z_0)\right]dz \\ &= Dz_0U_0 - \tfrac{1}{2}(w_*^2/v^m)B^2z_0^2 - \frac{z_0w_*}{\kappa}[t\ln t - t]_{1+B}^{1+D} \\ &= \tfrac{1}{2}Bz_0V_0 + (D-B)\frac{z_0w_*}{\kappa} - z_0(U_0 - V_0) \end{aligned} \tag{A7}$$

(extensive cancellations occur via the definitions (A2) and (A4)).

APPENDIX B: LOG PROFILE [CF. PLANT AND WRIGHT, 1980]

The log profile is given by

$$U(z) \equiv U_0 - \frac{w_*}{\kappa}\ln(1+z/z_0) \tag{B1}$$

(where fully turbulent flow is assumed). The effective drift is given by *Plant and Wright* [1980] rather than found via (3):

$$q \approx U_0 - U(0.044\lambda) \approx \frac{w_*}{\kappa}\ln(1+0.276/kz_0) \tag{B2}$$

where $\lambda = 2\pi/k$ is the wavelength. The drift momentum is given simply by (A7) with $B \equiv 0$:

$$M_0 = D\frac{z_0w_*}{\kappa} - z_0U_0 \tag{B3}$$

where D is as defined in (A4).

For use with the varying stress solution (via equation (61)) the momentum in the layer above $x^a \equiv 0.276/k$ is given by

$$M^a = z^a(U^a + w_*/\kappa) - z_0q_0 \tag{B4}$$

Finally, for use in computing the induced modulations, depth derivatives of q are also needed:

$$z_0\frac{\partial q}{\partial z_0} = k\frac{\partial q}{\partial k} = -\frac{kz_0(w_*/\kappa)}{kz_0/0.276 + 1} \tag{B5}$$

REFERENCES

Abramowitz, M., and I. Stegun, *Handbook of Mathematical Functions*, Dover, New York, 1965.

Alpers, W., and K. Hasselmann, The two-frequency microwave technique for measuring ocean-wave spectra from an airplane or satellite, *Boundary Layer Meteorol*, *13*, 215–230, 1978.

Alpers, W., and I. Hennings, A theory of the imaging mechanism of underwater bottom topography by real and synthetic aperture radar, *J. Geophys. Res.*, *89*(C6), 10529–10546, 1984.

Bretherton, F. P., and C. J. R. Garrett, Wavetrains in inhomogeneous moving media, *Proc. R. Soc. London, Ser. A*, *302*, 529, 1969.

Cox, C. S., Measurements of slopes of high-frequency wind waves, *J. Mar. Res.*, *16*, 199–225, 1958.

Garrett, C., and J. Smith, On the interaction between long and short surface waves, *J. Phys. Oceanogr.*, *6*, 925–930, 1976.

Gent, P. R., and P. A. Taylor, A numerical model of the air flow above water waves, *J. Fluid Mech.* *77*, 105–128, 1976.

Hsiao, S. V., and O. H. Shemdin, Measurements of wind velocity and pressure with a wave follower during Marsen, *J. Geophys. Res.*, *88*, 9841–9850, 1983.

Keller, W. C., and J. Wright, Microwave scattering and the straining of wind generated waves, *Radio Sci.*, *10*, 139–147, 1975.

Keller, W. C., W. J. Plant, and D. E. Weissman, The dependence of X band microwave sea return on atmospheric stability and sea state, *J. Geophys. Res.*, *90*, 1019–1029, 1985.

Landahl, M. T., J. A. Smith, and S. E. Widnall, The interaction between long and short wind-generated waves, paper presented at IUCRM Symposium on Wave Dynamics and Radio Probing of the Ocean Surface, Miami Beach, Fla., May 1981.

Lange, P. A., and H. Huhnerfuss, Horizontal surface tension gradients induced in monolayers by gravity water wave action, *J. Phys. Oceanogr.*, *14*, 1620–1628, 1984.

Larson, T. R., and J. Wright, Wind generated gravity-capillary waves: Laboratory measurements of temporal growth rates using microwave backscatter, *J. Fluid Mech.*, *70*, 417, 1975.

Longuet-Higgins, M. S., On wave breaking and the equilibrium spectrum of wind generated waves, *Proc. R. Soc. London, Ser. A*, *311*, 371–389, 1969*a*.

Longuet-Higgins, M. S., Action of a variable stress at the surface of water waves, *Phys. Fluids*, *12*, 737, 1969*b*.

Monaldo, F. M., and R. S. Kasevich, Measurement of short-wave modulation using fine time-series optical spectra, *J. Phys. Oceanogr.*, *11*, 1034–1036, 1981.

Monaldo, F. M., and R. S. Kasevich, Optical determination of short-

send's [1980] "rapid distortion" model of turbulence over a wind wave, though it is larger than the variations according to most other theories.

An interesting consequence of the implied stress modulation is an enhancement of the long-wave growth. By the analysis of *Garrett and Smith* [1976], it doesn't matter whether the stress is applied to the drift or the short waves; the net long-wave growth becomes

$$G^{LW} = G_0 + t_1\Omega(w_*/C^L)^2 = (33 + t_1)\Omega(w_*/C^L)^2 \quad (72)$$

Thus the long-wave growth rate might be nearly doubled by the input from the shear stress. This growth enhancement could "cut in" at some minimum wavelength, at which shorter waves become available for modulation (conceivably helping to explain the increased growth rate observed by *Plant and Wright* [1977] for waves longer than 10 cm or so). This nonresonant, nonlinear transfer is implied by the above model and does not affect further the short-wave amplitudes.

In the foregoing analysis there is no fundamental reason to exclude resonant nonlinear interactions. They are excluded primarily for simplicity, and also to preserve the independence of results for different wavelengths. Since waves on both sides of c^{min} are (presumably) modulated by the long waves, the strength of these interactions could also be modulated and hence contribute to the observed modulations. It is also likely that the differential advection of waves by the drift is important to the resonance condition, so that drift modulation could enter here as well. Since resonant interactions may have a gentler action dependence than the dissipation criterion employed above, their inclusion could "soften" the slope cutoff somewhat, yielding (for example) a slower relaxation of the short waves.

Consider also the turbulent nature of the drift layer. The critical slope (for example) should be regarded as random, and the dissipation rate should therefore take into account distributions of both wave slopes and critical slopes. In fact, coupling of the short waves and drift layer could be included by considering a joint distribution of wave- and critical-slopes. Note that the coevolution of the short waves and drift is an inherently nonlinear process, so that (for example) the whole spectrum of waves should be considered at once. Possibly (given the strong input to waves near c^{min}), only a relatively small band of short waves is important to the drift evolution. This might help account for the apparent "tuning" referred to above.

The possibility of other sources for short-wave action should not be neglected. Recently, I observed the sea surface under 10- to 15-m/s winds from aboard the R/V FLIP. I noted that relatively small scale whitecaps or "spills" frequently occur, directed mostly downwind but with some directional distribution (within about 20° to 30° off the wind). These spills occur more frequently near the dominant wave crests (commonly a bit ahead), but occasionally occur between crests as well. The effect of these small spills appears similar to that of dragging small objects along the surface, producing miniature "wakes" of short, centimeter-scale waves; thus in addition to removing energy from midscale waves, they can act as a source of very short waves, creating them preferentially near long-wave crests. This may contribute to the variations in the short-wave generation required to match the data, subsumed into t_1 in the foregoing.

The results of the above model should encourage further work. A suggestion is to regard the short "scatterers" as probes of the drift current. Since different wavelengths probe to different depths, an attractive possibility would be to "step" the radar frequency rapidly through several frequencies (with, say, a few microseconds cycle time) in order to probe several depths virtually at once. Alternatively, this "scanning" is already available in the optical technique of *Monaldo and Kasevich* [1981, 1982]. In addition to providing information about the structure of the drift current, this would provide in situ estimates of the spectral slope, and hence allow more accurate estimation of the 'spectral shifting' due to both straining and tilting.

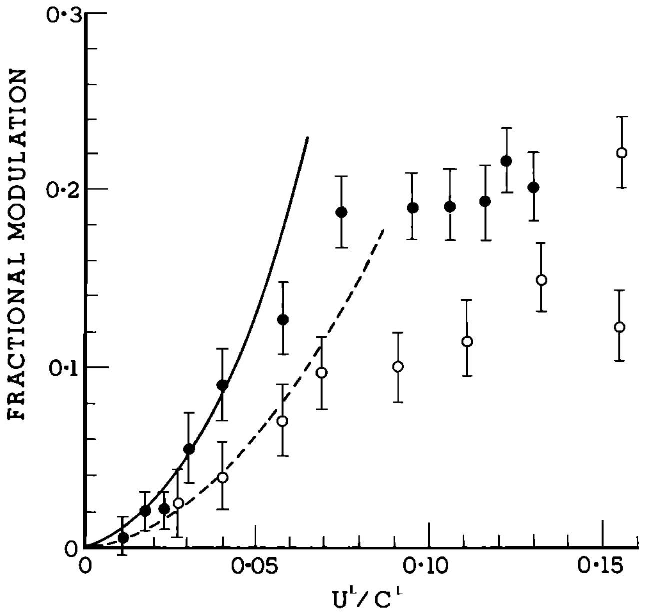

Fig. 14. Measured fractional modulation of 2.3-cm waves versus long-wave steepness U^L/C^L (looking upwind in a wave tank; long-wave frequency is 0.575 Hz). Solid points are for $u_* = 16.5$ cm/s; open points are for $u_* = 30$ cm/s. The curves correspond to Keller and Wright's first order relaxation model (figure reproduced from *Keller and Wright* [1975]).

7. CONCLUSIONS

A physical model including local growth and drift-enhanced dissipation can be made to agree crudely with observations of short surface waves, both in the wind dependence of the equilibrium steepness and the magnitude and phase of modulations by longer waves. The viability of this model depends on several illknown factors:

1. The depth scale z_0 of the drift must increase with windspeed (e.g., $z_0 \sim w_*$ or w_*^2).
2. The timescales of development of the short waves and drift current (to depth comparable to k) must be nearly the same. Thus a close tuning is implied between the drift current and short waves, suggesting active coupling between them. In any case, the drift is very important to the short-wave dynamics and should be studied further.
3. The implied source of the observed short-wave modulation is primarily variations in wind stress, rather than direct straining of either the waves or the drift current. The implied stress modulation is rather large, around 15 to 20 times the long-wave steepness, with the maximum stress just forward of the long-wave crests (on the upward accelerating face).

APPENDIX A: LOG LINEAR PROFILE

The log linear profile is defined by (with z increasing downward

$$\begin{aligned} U_0 - U(z) &= z(w_*^2/\nu^m) \qquad & z \le Bz_0 \\ U_0 - U(z) &= (w_*/\kappa)\ln(1 + z/z_0) \qquad & z > Bz_0 \end{aligned} \quad \text{(A1)}$$

wave modulation by long ocean gravity waves, *IEEE Trans. Geosci. Remote Sensing*, *GE-20*, 254–258, 1982.

Phillips, O. M., *The Dynamics of the Upper Ocean*, 2nd ed., 336 pp., Cambridge University Press, New York, 1977.

Phillips, O. M., On the response of short ocean wave components at a fixed wavenumber to ocean current variations, *J. Phys. Oceanogr.*, *14*, 1425–1433, 1984.

Phillips, O. M., and M. L. Banner, Wave breaking in the presence of wind drift and well, *J. Fluid Mech.*, *66*, 625–640, 1974.

Plant, W. J., On the steady-state energy balance of short gravity wave systems, *J. Phys. Oceanogr.*, *10*, 1340–1352, 1980.

Plant, W. J., A relationship between wind stress and wave slope, *J. Geophys. Res.*, *87*, 1961–1967, 1982.

Plant, W. J., and W. C. Keller, The two-scale radar wave probe and SAR imagery of the ocean, *J. Geophys. Res.*, *88*, 9776–9784, 1983.

Plant, W. J., and J. Wright, Growth and equilibrium of short gravity waves in a wind wave tank, *J. Fluid Mech.*, *82*, 767–793, 1977.

Plant, W. J., and J. Wright, Phase speeds of upwind and downwind travelling short gravity waves, *J. Geophys. Res.*, *85*, 3304–3310, 1980.

Plant, W. J., W. C. Keller, and A. Cross, Parametric dependence of ocean wave–radar modulation transfer functions, *J. Geophys. Res.*, *88*, 9747–9756, 1983.

Stewart, R. H., and J. W. Joy, HF radio measurements of surface currents, *Deep Sea Res.*, *21*, 1039–1049, 1974.

Tennekes, H., and J. L. Lumley, *A First Course in Turbulence*, 300 pp., MIT Press, Cambridge, Mass., 1972.

Thompson, T. W., D. E. Weissman, and F. I. Gonzalez, L-band radar backscatter dependence upon surface wind stress: A summary of new Seasat-1 and aircraft observations, *J. Geophys. Res.*, *88*, 1727–1735, 1983.

Townsend, A. A., The response of sheared turbulence to additional distortion, *J. Fluid Mech.*, *81*, 171–191, 1980.

Trowbridge, J., and O. S. Madsen, Turbulent wave boundary layers, 1, Model formulation and first-order solution, *J. Geophys. Res.*, *89*, 7989–7998, 1984.

Valenzuela, G. R., The growth of gravity-capillary waves in a coupled shear flow, *J. Fluid Mech.*, *76b*, 229–250, 1976.

Valenzuela, G. R., Theories for the interaction of electromagnetic and oceanic waves—A review, *Boundary Layer Meteorol.*, *13*, 61–85, 1978.

Valenzuela, G. R., An asymptotic formulation for SAR images of the dynamical ocean surface, *Radio Sci.*, *15*, 105–114, 1980.

Valenzuela, G. R., and M. B. Laing, Nonlinear energy transfer in gravity-capillary wave spectra with applications, *J. Fluid Mech.*, *54*, 507–520, 1972.

Valenzuela, G. R., and J. W. Wright, Modulation of short gravity-capillary waves by longer scale periodic flows—A higher order theory, *Radio Sci.*, *14*, 1099–1110, 1979.

Wright, J. W., A new model for sea clutter, *IEEE Trans. Antennas Propag.*, *AP-16*, 217–223, 1968.

Wright, J. W., W. J. Plant, W. C. Keller, and W. L. Jones, Ocean wave–radar modulation transfer functions from the West Coast experiment, *J. Geophys. Res.*, *85*, 4957–4966, 1980.

Wu, J., Wind-induced drift currents, *J. Fluid Mech.*, *68*, 49–70, 1975.

J. Smith, Marine Physical Laboratory, A-013, Scripps Institution of Oceanography, University of California, San Diego, La Jolla, CA 92093.

(Received September 27, 1985;
accepted September 30, 1985.)